



PUBLISHED FOR SISSA BY SPRINGER

RECEIVED: December 19, 2014

ACCEPTED: March 10, 2015

PUBLISHED: April 7, 2015

Search for physics beyond the standard model in dilepton mass spectra in proton-proton collisions at $\sqrt{s} = 8$ TeV



The CMS collaboration

E-mail: cms-publication-committee-chair@cern.ch

ABSTRACT: Dimuon and dielectron mass spectra, obtained from data resulting from proton-proton collisions at 8 TeV and recorded by the CMS experiment, are used to search for both narrow resonances and broad deviations from standard model predictions. The data correspond to an integrated luminosity of 20.6 (19.7) fb⁻¹ for the dimuon (dielectron) channel. No evidence for non-standard-model physics is observed and 95% confidence level limits are set on parameters from a number of new physics models. The narrow resonance analyses exclude a Sequential Standard Model Z'_{SSM} resonance lighter than 2.90 TeV, a superstring-inspired Z'_ψ lighter than 2.57 TeV, and Randall-Sundrum Kaluza-Klein gravitons with masses below 2.73, 2.35, and 1.27 TeV for couplings of 0.10, 0.05, and 0.01, respectively. A notable feature is that the limits have been calculated in a model-independent way to enable straightforward reinterpretation in any model predicting a resonance structure. The observed events are also interpreted within the framework of two non-resonant analyses: one based on a large extra dimensions model and one based on a quark and lepton compositeness model with a left-left isoscalar contact interaction. Lower limits are established on M_5 , the scale characterizing the onset of quantum gravity, which range from 4.9 to 3.3 TeV, where the number of additional spatial dimensions varies from 3 to 7. Similarly, lower limits on Λ , the energy scale parameter for the contact interaction, are found to be 12.0 (15.2) TeV for destructive (constructive) interference in the dimuon channel and 13.5 (18.3) TeV in the dielectron channel.

KEYWORDS: Hadron-Hadron Scattering, Beyond Standard Model, Particle and resonance production

ARXIV EPRINT: [1412.6302](https://arxiv.org/abs/1412.6302)

Contents

1	Introduction	1
2	The CMS detector	3
3	Methodology	3
4	Event selection	4
4.1	Triggers	4
4.2	Lepton reconstruction and identification	5
4.3	Study of energy deposits in the ECAL crystals	7
5	Background sources	8
5.1	The Z/γ^* background	9
5.2	Other background sources with prompt lepton pairs	9
5.3	Events with misidentified and non-prompt leptons	9
5.4	Cosmic ray muon backgrounds	11
6	Dilepton invariant mass spectra	11
7	Statistical analysis and results	12
7.1	Resonance search	12
7.2	Resonance search likelihood function	16
7.3	Non-resonant searches	17
7.4	Non-resonant likelihood function	17
7.5	Uncertainties	17
7.6	Exclusion limits	18
8	Summary	25
	The CMS collaboration	31

1 Introduction

This paper describes a general investigation for evidence of physics beyond the standard model (SM) using the dilepton (dimuon and dielectron) invariant mass spectra obtained from $\sqrt{s} = 8$ TeV proton-proton (pp) collision data collected by the CMS detector at the CERN LHC [1]. The analyses include searches both for new narrow resonances and for deviations from SM expectations at high invariant mass values that do not result in a resonance structure.

Numerous new physics models predict the existence of narrow resonances at the TeV mass scale. The approach described in this paper is designed to be independent of specific model assumptions, allowing the results to be reinterpreted for any model predicting a spin-1 or spin-2 narrow resonance. A generic resonance is denoted by Z' in this paper; wherever a specific model is implied a subscript is used to specify the model. The search results are interpreted in the context of various models: the Sequential Standard Model Z'_{SSM} with SM-like couplings [2], the Z'_ψ possible in grand unified theories where the gauge group is E_6 [3, 4], and Kaluza-Klein graviton (G_{KK}) excitations arising in the Randall-Sundrum (RS) model of extra dimensions [5, 6]. For a resonance mass of 2.5 TeV, the widths of the Z'_{SSM} and Z'_ψ are 80 and 14 GeV. Similarly, the G_{KK} widths are 3.5, 9.0, and 35 GeV for G_{KK} coupling parameters $k/\overline{M}_{\text{Pl}}$ of 0.01, 0.05, and 0.10, where k is the warp factor of n -dimensional anti-de Sitter space and \overline{M}_{Pl} is the reduced Planck scale.

Non-resonant deviations from the SM are interpreted within two frameworks: the (1) Arkani-Hamed-Dimopoulos-Dvali (ADD) model [7, 8], where possible enhancements in the high invariant mass cross section are due to virtual graviton-mediated processes, and (2) contact interactions, specifically the left-left isoscalar model [9], where possible deviations are due to quark and lepton substructures.

In the ADD model, three possible parametrizations of the differential cross section are given by Hewett [10], Han, Lykken, Zhang (HLZ) [11], and Giudice, Rattazzi, Wells (GRW) [12]. In the HLZ convention, the parameters that define the characteristics of the model are the ultraviolet cutoff scale of the divergent sum of the KK graviton excitations M_S , which characterizes the onset of quantum gravity effects [13], and the number of extra spatial dimensions n_{ED} . These can be related to the similar ultraviolet cutoff scale Λ_T in the GRW convention:

$$\Lambda_T^{-4} = \begin{cases} M_S^{-4} \log\left(\frac{M_S^2}{M_{\ell\ell}^2}\right), & n_{\text{ED}} = 2; \\ \frac{2}{n_{\text{ED}}-2} M_S^{-4}, & n_{\text{ED}} > 2, \end{cases} \quad (1.1)$$

where $M_{\ell\ell}$ is the dilepton invariant mass. The HLZ and GRW conventions are based on effective field theory, which is expected to break down at the energy scale M_{max} at which quantum gravity effects become strong, i.e. close to M_S (HLZ) or Λ_T (GRW). In this analysis, when presenting results in the HLZ (GRW) convention it is assumed that M_{max} is equal to M_S (Λ_T). The results do not depend strongly on the exact choice of M_{max} for a broad range of M_{max} values around the chosen cutoff scale [14].

The data are also interpreted in the context of possible contact interactions (CI). The existence of three families of quarks and leptons might be explained if these particles are composed of more fundamental constituents. In order to confine the constituents and to account for the properties of quarks and leptons, a new strong gauge interaction, metacolor, is introduced. Below a given interaction energy scale Λ , the effect of the metacolor interaction is to bind the constituents into metacolor-singlet states. For parton-parton centre-of-mass energies less than Λ , the metacolor force will manifest itself in the form of a flavour-diagonal CI [15]. The model considered here is the left-left isoscalar model, which is the conventional benchmark for CI in the dilepton channel. The predicted differential

cross section includes an interference term, which may be positive or negative, and the measurements are interpreted in the context of both possibilities.

Results of searches for narrow $Z' \rightarrow \ell^+ \ell^-$ ($\ell = \mu, e$) resonances in pp collision data have previously been reported by the ATLAS and CMS Collaborations [16, 17]. The CDF and D0 Collaborations have published results based on a $p\bar{p}$ collision sample at $\sqrt{s} = 1.96$ TeV and $\approx 5 \text{ fb}^{-1}$ of integrated luminosity [18–23]. Similarly, there are recent limits from the LHC on the ADD [14, 24] and CI [24–28] model parameters in dilepton channels.

The results presented in this paper are obtained from an analysis of a data sample collected in 2012 at $\sqrt{s} = 8$ TeV, corresponding to an integrated luminosity of 20.6 (19.7) fb^{-1} for the dimuon (dielectron) channel. The data used have been processed with the most recent calibration and alignment constants for all detector elements.

2 The CMS detector

The central feature of the CMS detector is a superconducting solenoid providing an axial magnetic field of 3.8 T and enclosing the all-silicon inner tracker, the crystal electromagnetic calorimeter (ECAL), and the brass and scintillator hadron calorimeter (HCAL). The inner tracker is composed of a silicon pixel detector and a silicon strip tracker, and measures charged-particle trajectories in the pseudorapidity range $|\eta| < 2.5$. The finely segmented ECAL consists of nearly 76 000 lead tungstate crystals, which provide coverage in pseudorapidity up to $|\eta| = 3.0$. The muon system covers the pseudorapidity region $|\eta| < 2.4$ and consists of up to four stations of gas-ionization muon detectors installed outside the solenoid and sandwiched between the layers of the steel flux-return yoke. A more detailed description of the CMS detector, together with a definition of the coordinate system used and the relevant kinematic variables, can be found in ref. [29].

The CMS experiment uses a two-level trigger system. The level-1 (L1) trigger [30], composed of custom hardware processors, selects events of interest using information from the calorimeters and muon detectors and reduces the readout rate from the 20 MHz bunch-crossing frequency to a maximum of 100 kHz. The high level trigger (HLT) [31] uses software algorithms accessing the full event information, including that from the inner tracker, to reduce further the event rate to the 400 Hz that is recorded.

3 Methodology

The searches described in this paper probe fundamentally different manifestations of physics beyond the standard model. The first type looks for a resonance structure appearing above a smooth background. This search parametrizes the expected signal and background shapes using appropriate functional forms and takes an unbinned likelihood approach to establish compatibility with the representative new physics models used as benchmarks. The second type looks for a smooth deviation from the background where no resonance structure is expected. In the non-resonant analyses the number of events above a particular invariant mass is compared with the total number of expected background events. The same observed mass spectra are used by all of the analyses.

To be robust against uncertainties in the absolute background level, the search for resonances makes use only of the shape of the dilepton mass spectra. In the absence of a signal, limits are set on the ratio R_σ of the production cross section times branching fraction for high-mass resonances to that of the Z boson. In this approach, many experimental and theoretical uncertainties common to both measurements cancel or are reduced. The non-resonant analyses also use the number of reconstructed Z boson events to reduce some systematic uncertainties. Using theoretical cross sections, lower mass limits, or limits on model parameters in the case of the non-resonant analyses, are calculated for specific models. The experimental limits derived within the resonance analysis are designed to be easily reinterpretable in the context of any model predicting a narrow resonance, and spin-specific parametrizations for the product of the acceptance and the reconstruction efficiencies are provided for completeness. Similarly, the signal cross section limits above different lower mass thresholds may be reinterpreted in the context of other models predicting a non-resonant enhancement at large masses in the dilepton mass spectrum.

4 Event selection

4.1 Triggers

The trigger used to select dimuon events requires at least one muon candidate with transverse momentum $p_T > 40$ GeV. The candidate muon tracks in the HLT are created by combining tracks reconstructed using muon chamber information alone with information from the silicon tracking detectors. To keep the trigger rate at an acceptable level, the acceptance of this trigger is restricted to a pseudorapidity range of $|\eta| < 2.1$. In addition, the candidate tracks are required to have a $\chi^2/\text{dof} < 20$ and to have a point of closest approach to the beam axis of less than 0.1 cm in the transverse plane.

The trigger used to select dielectron events requires the presence of two clusters in the ECAL, each associated with a track reconstructed using tracker information. The clusters are reconstructed by summing energy deposits in crystals surrounding a “seed”, which is locally the crystal containing the largest energy. The summing procedure encompasses energy deposits potentially arising from bremsstrahlung emission. The clusters are required to have transverse energies $E_T (= E \sin(\theta))$ greater than 33 GeV. The total energy in the hadron calorimeter cells, within a cone of radius $\Delta R = \sqrt{(\Delta\eta)^2 + (\Delta\phi)^2} < 0.14$ centred on the ECAL cluster, is required to be less than 15% (10%) of the cluster energy in the barrel (endcap) region of the ECAL. At least one of the ECAL clusters identified in the HLT is required to be compatible with an energy deposit identified by the L1 trigger. In the electron trigger, ECAL cluster information is used to identify associated hits in the pixel detector, which are then used to initiate track reconstruction.

The trigger efficiencies can be represented as a product of uncorrelated efficiencies of the different trigger components. In order to determine these separate elements, various triggers with criteria different from those used for the signal triggers are employed. In general, these triggers have larger rates than the signal triggers and are prescaled, meaning that only a fraction of the events potentially passing these triggers are recorded. The tag-

and-probe methodology described in refs. [16, 32, 33] is used, where applicable, to obtain detailed efficiencies for the main contributions to the total efficiency.

The efficiency of a single muon trigger varies as a function of η , resulting in an efficiency for triggering on a dimuon system that varies between 97 and 100%. From simulations this efficiency is constant over the mass range from the region of the Z peak to greater than 3 TeV.

The total electron trigger efficiency, for events with two electron candidates that pass the offline electron selection requirements, is $(99.3 \pm 0.1)\%$ for $E_T > 38$ GeV, where the trigger efficiency reaches a plateau. Where required in the dielectron resonance analysis, and in the plots relevant to electrons shown in this paper comparing predicted event yields with data, the effect of trigger efficiencies on simulated event samples is included by using the trigger efficiencies determined from the data and applying a weight to each simulated event. In the ADD and CI analyses a systematic uncertainty is assigned to account for the small inefficiency.

4.2 Lepton reconstruction and identification

Muons and electrons are reconstructed using standard algorithms, described in more detail in refs. [16, 32, 33]. The primary vertices in the event are reconstructed using silicon tracker information [34]. In each analysis, the primary vertex closest to the origin of the reconstructed pair of leptons is used.

Muon tracks are reconstructed separately in both the muon system and the silicon tracker. For each compatible pair of tracks the set of space points is fitted to form a track that spans the entire detector [33]. For muons with $p_T < 200$ GeV, the transverse momentum resolution is dominated by the resolution on track parameters in the inner tracker [33]. However, above 200 GeV the muon stations also contribute significantly to the precision of the measurement. The muon p_T resolution is estimated using collision data and cosmic rays to be around 2% for $p_T \approx 100$ GeV and better than 10% for $p_T \approx 1$ TeV, for muons reconstructed in the barrel. Monte Carlo simulations reproduce the performance observed in collision data and cosmic rays. Each of the muon candidates is required to have $p_T > 45$ GeV and $\delta(p_T)/p_T < 0.3$, where $\delta(p_T)$ is the uncertainty in the measured p_T of the track. The muons must lie within the acceptance of the muon detectors, $|\eta| < 2.4$, furthermore the muon that triggers the event must be within $|\eta| < 2.1$ as a consequence of the trigger criteria. The muon candidates are required to have a transverse impact parameter of less than 0.2 cm with respect to the primary vertex position, at least one hit in the pixel detector, hits in at least six silicon-strip tracker layers, and matched segments in two or more muon stations. To suppress backgrounds from non-prompt muons, the scalar sum of the p_T of all other tracks with a z impact parameter within 0.2 cm of the relevant primary vertex and lying within a cone of $\Delta R < 0.3$ about the track of the muon candidate, is required to be less than 10% of the p_T of the candidate. The impact parameter criterion also reduces the effect of tracks originating from additional pp interactions occurring in the same bunch crossing (pileup) on reconstructed quantities. Its effectiveness was assessed using muons arising from Z bosons where efficiencies have been shown to agree in data and

simulation. When varying the average number of pileup events between 0 and 30 a change of less than 1% is observed in the muon selection efficiency.

Clusters in the ECAL are matched to hits in the silicon pixel detector, which are then used to seed tracks in the rest of the tracker. The resulting cluster-track matched pairs form electron candidates. These candidates are required to have $E_T > 35$ GeV and $|\eta| < 2.5$, excluding the barrel-endcap transition region $1.442 < |\eta| < 1.560$. To suppress the misidentification of jets as electrons, the sum of the p_T of all other tracks in a cone of $\Delta R < 0.3$ around the track of the electron candidate is required to be less than 5 GeV, which imposes an isolation condition on the track. To be used in the calculation of the isolation of the candidate track, the tracks have to be within 0.2 cm, in the z direction, of the primary vertex with which the electron candidates are associated. This requirement reduces the impact of pileup. For electrons with transverse energies above 100 GeV, a negligible change in the selection efficiency is observed as the number of pileup events increases from 0 to 40. For electrons identified as arising from Z bosons, i.e. where the E_T are much lower than 100 GeV, the efficiency falls by between 5 and 10% depending on the region of the detector in which the electrons are detected. Within this same cone, the sum of the E_T of the energy deposits in the calorimeter that are not associated with the candidate is required to be less than 3% (plus a small η -dependent offset) of the candidate E_T . This sum, which allows a selection on the isolation of the electron candidate, is corrected for the average energy density in the event [35] to minimize the dependence of the efficiency of this selection criterion on pileup. Further suppression of the misidentification of jets as electrons is achieved by requiring that the profile of the energy deposition in the ECAL be consistent with that expected for an electron, and that the sum of HCAL energy deposits in a cone of $\Delta R < 0.15$ be less than 5% of the ECAL energy of the electron. The track associated with the cluster is required to have no more than one hit missing in the pixel layers, and in the transverse plane to lie within 0.02 cm (barrel) or 0.05 cm (endcaps) of the primary vertex associated with the candidates. The energy resolution for the selected electrons varies between approximately 1.0 and 3.5% depending on the momentum, the extent of bremsstrahlung emission and the point of incidence on the ECAL [36].

For signal events, the total efficiency (including triggering, reconstruction, and identification) is estimated from simulated events. In the resonance analysis, limits are set on R_σ , which is the ratio of the product of cross section and branching fraction for Z' production relative to that for Z bosons. In the non-resonant analyses the relevant ratio is the one between the summed events above the minimum mass threshold and the number of events in the Z peak region. Therefore the simulation does not need to reproduce the absolute value of the efficiency in data; it must however correctly reproduce the evolution of the efficiency with E_T . Data are used to measure the electron identification efficiency at the Z resonance, using the tag-and-probe method [16, 32, 33]. The ratio of this efficiency to that found in simulation is 0.997 ± 0.007 for electrons in the barrel region and 0.979 ± 0.006 in the endcaps. This ratio was also studied as a function of the probe electron E_T to ~ 500 GeV and as a function of the tag-and-probe pair mass up to ~ 1 TeV, and was found to be invariant with respect to these quantities, although the systematic and statistical uncertainties become large at high transverse energies and masses. Using these scale factors,

the total efficiency to reconstruct and select electrons with $p_T > 100$ GeV is expected to be $(88 \pm 2)\%$ in the barrel region and $(84 \pm 4)\%$ in the endcaps, where the uncertainties cover the extrapolation of the data-to-simulation ratio to very high transverse momenta. This gives efficiencies for electron pairs of 78% where both electrons are in the barrel and 75% where one of the electrons is in the endcap. A similar procedure is used to evaluate the muon identification efficiency. Applying the tag-and-probe technique to muons from Z boson decays, and using tracks in the silicon inner tracker as probes, the total muon identification efficiency (including isolation) is measured to be $(95 \pm 1)\%$ in the barrel and endcap regions. The corresponding efficiency ratios between data and the simulation are 0.990 ± 0.005 and 0.993 ± 0.005 , respectively. To within the statistical precision available using the 2012 data sample, both the efficiencies and the related correction factors remain constant up to a p_T of approximately 300 GeV. With these correction factors applied, the combined reconstruction and selection efficiency for triggered events in the acceptance region is expected to be $(89 \pm 2)\%$ at a mass of 200 GeV. The simulation predicts that the efficiency above 200 GeV is constant to within 3%.

For both the dimuon and dielectron final states, two isolated, same-flavour leptons that pass the lepton identification criteria described above, are required. In the case of muons, the particle momentum is measured from the curvature of the associated track, and thus the sign of the charge is automatically determined. Muons in dimuon events are therefore required to have charges of opposite sign. Dielectron events are separated into barrel-barrel and barrel-endcap categories, because of the different signal-to-background ratios and mass resolutions in the two regions. The measurement of the energy of the electron depends only upon the energy deposition in the ECAL and therefore is independent of the charge of the particle. The opposite-sign requirement is therefore not applied to dielectron events since this would only result in a loss of efficiency without providing useful background suppression.

Muon candidates are also required to originate from the same vertex, by requiring the χ^2/dof to be less than 10 when tracks are fitted to a common vertex. Cosmic ray and beam halo muons are suppressed to negligible levels by the common-vertex requirement together with the further requirement that the opening angle between the two reconstructed muons be less than $\pi - 0.02$ radians.

The acceptance times efficiency for heavy particles with spins 1 and 2 decaying to lepton pairs is determined using simulation and varies as a function of the particle mass. Table 1 lists the parametrizations of the acceptance times efficiency as a function of mass along with their evaluation at two example mass points, 1000 and 2500 GeV. The uncertainties in this table are dominated by the uncertainties in the efficiencies described above.

4.3 Study of energy deposits in the ECAL crystals

The energy calibration procedure for the crystals in the ECAL makes use of both collision data and test beam data taken before the installation of the detector [29]. This procedure provides a well-calibrated detector up to energies of around 100 GeV. Very high energy electrons can potentially deposit energies of several hundreds of GeV in a single crystal.

Functional form		Acceptance×Efficiency		Uncertainty
		1000 GeV	2500 GeV	
spin 1				
$\mu^+\mu^-$	$0.81 - \frac{1.5\times 10^8}{(m+570)^3}$	0.77	0.80	3%
ee barrel-barrel	$0.59 - \frac{2.9\times 10^5}{m^2+7.5\times 10^5}$	0.43	0.55	4%
ee barrel-endcap	$0.06 - \frac{159}{m+345} + \frac{7.3\times 10^5}{m^2+1.8\times 10^6}$	0.21	0.10	6%
spin 2				
$\mu^+\mu^-$	$0.75 + \frac{112}{m-104} - \frac{6.1\times 10^4}{m^2+1.6\times 10^4}$	0.82	0.79	3%
ee barrel-barrel	$0.57 - \frac{3.0\times 10^4}{m^2+1.3\times 10^5}$	0.54	0.57	4%
ee barrel-endcap	$-0.24 + \frac{1.2\times 10^4}{m+3.5\times 10^4} + \frac{6.6\times 10^4}{m^2+7.5\times 10^5}$	0.13	0.09	6%

Table 1. Parametrizations of the product of the acceptance and the efficiency as a function of the mass m expressed in units of GeV.

The procedure described below was developed in order to ensure that the calibration could be extrapolated to such energies.

An electron deposits its energy over an array of crystals approximately 5×5 in extent. In general, only the energy deposited in the central crystal will significantly exceed the energies at which calibrations are performed. Given the shape of the electromagnetic shower, the energy of the central crystal can be predicted from the energy distribution in the surrounding 24 crystals. This is done using both an algorithmic fit to the distributions and an artificial neural network. The difference between the observed energy E_1 in the central crystal and the energy reconstructed, E_1^{rec} , is calculated from data using the above method. The distribution $(E_1 - E_1^{\text{rec}})/E_1$ obtained using simulated data results in a displacement from zero of the mean of the distribution of less than 0.01. For electrons in the data with energies above 500 GeV, the distribution found using simulation agrees with that for the data, where displacements of the mean are observed to be less than 0.01 in both the barrel and endcap regions. This procedure has also been adapted to reconstruct the energies in any crystals in a cluster where the readout is not functioning. This correction is used in about 2% of events where the dilepton mass is above 200 GeV.

5 Background sources

The principal standard model process that contributes to the dimuon and dielectron invariant mass spectra, either directly or via $\tau\tau$, is Drell-Yan production (Z/γ^*). There are also contributions from $t\bar{t}$, tW , and diboson processes. In addition, jets may be misidentified as leptons and contribute to the dilepton invariant mass spectra through multijet and vector boson plus jets final states. The contribution from diphotons misidentified as dielectrons has been established to be negligible.

5.1 The Z/γ^* background

Drell-Yan production is simulated using the POWHEG (r1513) [37–39] next-to-leading order (NLO) event generator. The differential cross section from this source can be modified by higher-order corrections and by variations in Parton Distribution Functions (PDF). Uncertainties due to these sources are included in all of the analyses and are described in section 7.5. The resonance search relies only on the shape of the spectrum, using data primarily from mass regions where no non-standard-model contribution is expected, to constrain the magnitude of the background, making the result insensitive to the predicted absolute cross section. The non-resonant analyses use simulation to predict the number of events and hence are more sensitive to these systematic uncertainties.

5.2 Other background sources with prompt lepton pairs

Prompt lepton pairs can result from $t\bar{t}$, tW , and diboson production in addition to the dominant Drell-Yan process. In order to demonstrate that simulations provide a good representation of these processes, their flavour-symmetric nature is exploited. The $e^\pm\mu^\mp$ invariant mass spectrum is used solely to test the quality of the simulations. The $t\bar{t}$ and tW simulated samples are generated using POWHEG [40], while the diboson simulated samples are generated using the PYTHIA v6.426 [41] event generator.

Figure 1 shows the $e^\pm\mu^\mp$ invariant mass spectrum resulting from a trigger that requires the presence of both a muon and an electromagnetic object. The muon and electron selection criteria described in section 4 are used and the leptons are required to have opposite signs. All components are estimated from simulations except for the component arising from multijet events where both lepton candidates are misidentified jets. This component is derived from data by using the same-sign $e\mu$ spectrum. The observed number of opposite-sign $e\mu$ events is 20 513 (6756) in the mass region above 120 (200) GeV. Using simulations, and the estimation from data for the contribution from jets being misreconstructed as leptons, the expected number of events above 120 (200) GeV is $21\,100 \pm 600$ (6800 ± 200).

5.3 Events with misidentified and non-prompt leptons

Both jets and photons can be misidentified as prompt electrons. Potential sources of such backgrounds are $W(\rightarrow e\nu)+\text{jets}$, $\gamma+\text{jets}$, and multijet events. The method described below primarily uses the data to determine the contribution to the observed mass spectra from these sources. The misidentification rate (MR) is the probability for a jet, having been reconstructed as an electron candidate, to pass the electron selection. This rate is measured using a sample collected with a prescaled single electromagnetic cluster trigger. To suppress the contribution from Z boson decays, events in this sample are required to have no more than one reconstructed electron above 10 GeV. Contamination from genuine electrons in $W+\text{jet}$ events and from converted photons in $\gamma+\text{jet}$ events may affect the MR measurement. A less significant source of contamination is from processes that can give a single electron such as $t\bar{t}$, tW , WW , WZ , $Z/\gamma^* \rightarrow \tau^+\tau^-$, and $Z/\gamma^* \rightarrow e^+e^-$, and in which a second electron is produced but fails to be reconstructed. The effect of the real electromagnetic

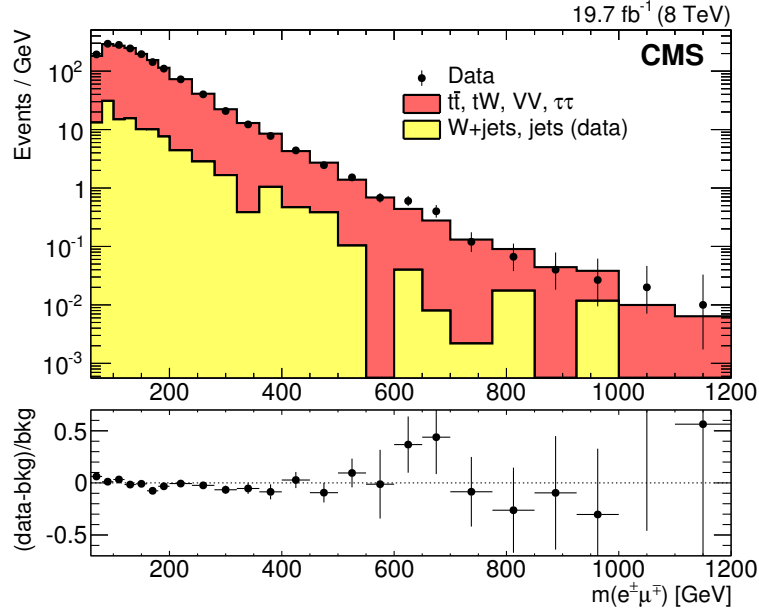


Figure 1. The observed opposite-sign $e^\pm\mu^\mp$ dilepton invariant mass spectrum (data points). The filled red (dark shading) histogram shows the contribution to the spectrum from $t\bar{t}$ and other sources of prompt leptons (tW , diboson production, $Z/\gamma^* \rightarrow \tau^+\tau^-$, W +jets, jets). The background where at least one of the reconstructed objects is not a correctly identified lepton is shown in yellow (light shading). All components are estimated using simulations except for the jet component where both leptons are misidentified jets, which is estimated from the data using the same-sign $e^\pm\mu^\pm$ spectrum. The simulated backgrounds are normalized so that in the dielectron channel, the observed data and the prediction from simulation agree in the region of the $60 < m_{ee} < 120$ GeV. The lower plot shows the difference between the number of data and background events in each bin divided by the number of background events. All error bars shown are statistical only.

object contamination on the MR is corrected using simulated samples where the W +jet simulated sample is generated using MADGRAPH 5 [42] and the γ +jet sample is derived from the PYTHIA event generator. Following these corrections, the MR is defined as the number of electrons passing the full selection divided by the number of electron candidates in the sample. The misidentification rate is quantified in bins of E_T and η .

Once this rate has been measured, the jet background can be estimated using two samples selected from data. The first sample consists of events with two reconstructed electron candidates that pass the trigger, but fail the full selection. The second sample is similar to the first sample except one electron has to pass the full selection instead of failing it. When weighted by the $MR/(1 - MR)$ appropriate for each electron, the first sample estimates the multijet component, where both electrons candidates arise from misidentified jets, of the jet background only. When weighted by the $MR/(1 - MR)$ appropriate for the failing electron, the second sample estimates the sum of the $W \rightarrow e\nu$ +jet background, γ +jet background, and twice the multijet background. The second sample overestimates the multijet background by a factor of two because there are two combinations possible with one electron passing and one failing the selection. However, as the multijet back-

ground has been estimated by the first sample, the total jet background is the number of events estimated from the second sample minus the number of events estimated from the first sample. Based on the results of various consistency tests and cross-checks, a 40% systematic uncertainty is applied to the misidentified-jet background estimate. The estimated background contributions are shown in table 3.

In principle the dimuon channel also has contributions from jets and photons that are misidentified as muons. However, the background from this source, determined using the procedure in ref. [16], is found to be negligible as can be seen in table 2.

5.4 Cosmic ray muon backgrounds

The potential background in the $\mu^+\mu^-$ sample from events containing cosmic ray muons is suppressed by the selection criteria described in section 4.2, which reject events with back-to-back muons and events with muons that have a large impact parameter relative to the collision vertex. For the dimuon mass region $m_{\mu\mu} > 200$ GeV, the residual expected background is estimated using two event samples. Events in one sample are selected without imposing the requirement on the dimuon opening angle and in the other sample the requirements on muon impact parameter and on the existence of a good quality primary vertex are not applied. The efficiencies of the remaining selection requirements are estimated using these samples under the assumption that they are uncorrelated. The background due to cosmic rays is estimated to be less than 0.1 events above a mass of 200 GeV.

6 Dilepton invariant mass spectra

The dilepton invariant mass spectra are shown in figures 2 and 3, where the data are compared with the expected backgrounds. If more than two leptons passing all selection criteria are present in an event, the pair with the largest invariant mass is chosen. The largest dimuon invariant mass observed is 1840 GeV and the largest dielectron mass is 1790 GeV. In figures 2 and 3 the contribution labeled “Jets” consists of events where at least one jet has been misreconstructed as a lepton. The other background components are derived from simulations. The relative fractions of the simulated processes are fixed by their theoretical cross sections, and the total simulated background contribution is normalized to the number of events in the data in the region of $60 < m_{\ell\ell} < 120$ GeV. The $p_T > 45$ GeV selection requirement on the muons removes most of the events in this mass range, and also has a significant effect on the efficiency of events above this mass region (but well below the search region of interest). To derive the normalization for dimuon production, a prescaled trigger, which is identical to the main muon trigger but with a lower p_T selection criterion, is used to select events. The use of this trigger allows the offline p_T threshold criterion to be lowered to 27 GeV. Figure 4 shows the corresponding cumulative distributions of the spectra. The SM expected yields in various mass bins are shown compared to the observed yields in tables 2 and 3. These plots and the tables illustrate that there is good agreement between observation and expectation in the whole explored region including dilepton masses above 1 TeV. The analyses are designed to look for evidence of beyond the

$m_{\mu\mu}$ range (GeV)	Data	Total background	Z/γ^*	$t\bar{t}$ + other prompt bkgd	Jet mis- reconstruction
120–400	96299	96800 ± 4300	86800 ± 3800	9900 ± 420	147 ± 18
400–600	1367	1460 ± 80	1180 ± 60	276 ± 13	3 ± 3
600–900	273	283 ± 19	246 ± 16	37 ± 4	—
900–1300	55	46 ± 4	40 ± 4	5 ± 1	—
1300–1800	8	6.1 ± 0.8	5.7 ± 0.8	0.4 ± 0.2	—
>1800	2	0.8 ± 0.2	0.8 ± 0.2	—	—

Table 2. The number of dimuon events in various invariant mass ranges for an integrated luminosity of 20.6 fb^{-1} . The total background is the sum of the events for the standard model processes listed. The yields from simulation are normalized relative to the expected cross sections, and overall the simulation is normalized to the data using the number of events in the mass window 60–120 GeV acquired using a prescaled low threshold trigger. Uncertainties include both statistical and systematic components, summed in quadrature. A dash (—) is used to indicate negligibly small contributions.

m_{ee} range (GeV)	Data	Total background	Z/γ^*	$t\bar{t}$ + other prompt bkgd	Jet mis- reconstruction
120–400	87117	88700 ± 3900	77100 ± 3900	10130 ± 680	1500 ± 300
400–600	1266	1240 ± 100	970 ± 100	226 ± 15	40 ± 8
600–900	259	245 ± 21	211 ± 21	27 ± 2	7 ± 1
900–1300	41	39 ± 3	35 ± 3	3.5 ± 0.2	1.2 ± 0.2
1300–1800	4	5.2 ± 0.5	4.8 ± 0.5	0.36 ± 0.02	0.005 ± 0.001
>1800	0	0.64 ± 0.06	0.64 ± 0.06	—	—

Table 3. The number of dielectron events in various invariant mass ranges for an integrated luminosity of 19.7 fb^{-1} . The total background is the sum of the events for the standard model processes listed. The yields from simulation are normalized relative to the expected cross sections, and overall the simulation is normalized to the data using the number of events in the mass window 60–120 GeV. Uncertainties include both statistical and systematic components, summed in quadrature. A dash (—) is used to indicate negligibly small contributions.

standard model physics that is expected to become manifest at masses above about 1 TeV, nonetheless the entire region above masses of 200 GeV is examined for such evidence.

7 Statistical analysis and results

The observed invariant mass spectra agree with expectations based on standard model processes. Limits have been set on the possible presence of the narrow heavy resonances predicted in various models, and on the excesses of the form expected in the ADD and CI models. The procedures used are described in the following sections.

7.1 Resonance search

An unbinned likelihood Bayesian approach is used to set 95% confidence level (CL) cross section limits on possible contributions for narrow heavy resonances.

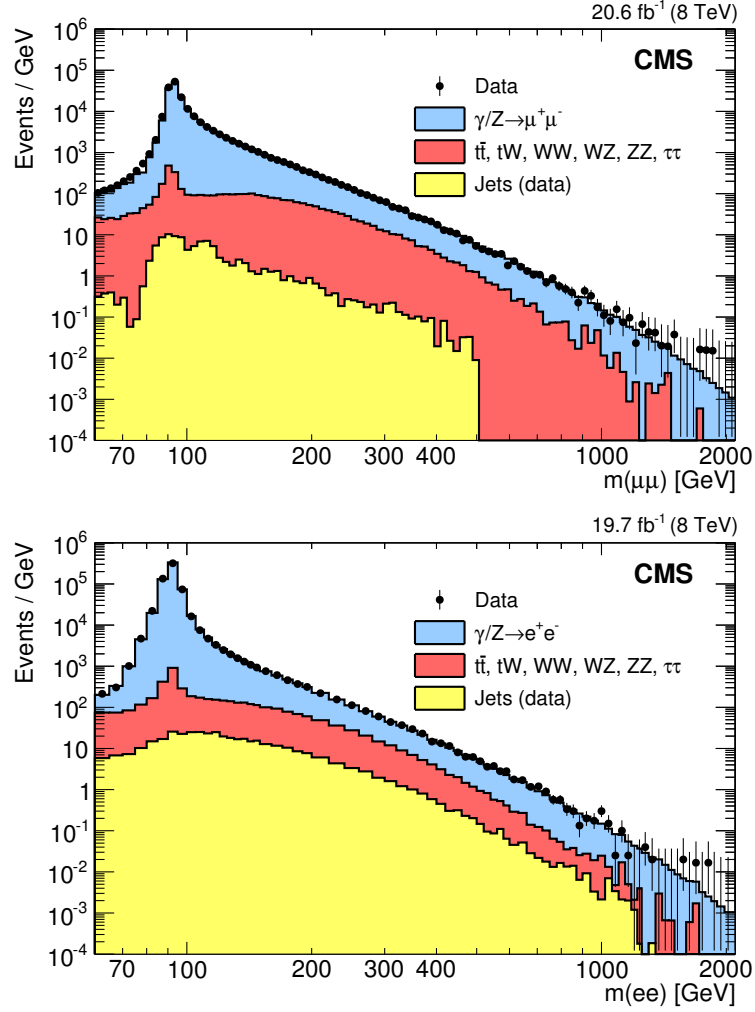


Figure 2. The invariant mass spectrum of $\mu^+\mu^-$ (top) and ee (bottom) events. The points with error bars represent the data. The histograms represent the expectations from SM processes: Z/γ^* , $t\bar{t}$, and other sources of prompt leptons (tW , dibosons, $Z/\gamma^* \rightarrow \tau^+\tau^-$), as well as the multijet backgrounds. Multijet backgrounds contain at least one jet that has been misreconstructed as a lepton. The simulated backgrounds are normalized to the number of events in the data in the region of $60 < m_{\ell\ell} < 120$ GeV, with the dimuon channel using events collected with a prescaled lower-threshold trigger.

The parameter of interest is the ratio of the cross sections for producing dilepton final states:

$$R_\sigma = \frac{\sigma(\text{pp} \rightarrow Z' + X \rightarrow \ell\ell + X)}{\sigma(\text{pp} \rightarrow Z + X \rightarrow \ell\ell + X)}. \quad (7.1)$$

The use of this ratio R_σ eliminates the uncertainty in the integrated luminosity and reduces the dependence on the experimental acceptance, trigger, and offline efficiencies. The ratio of acceptances of a new boson to that of the Z boson are calculated using simulations. This has been done for two possible scenarios, corresponding to spin 1 or 2 final states. The dimuon and dielectron channels are treated separately. The cross sections

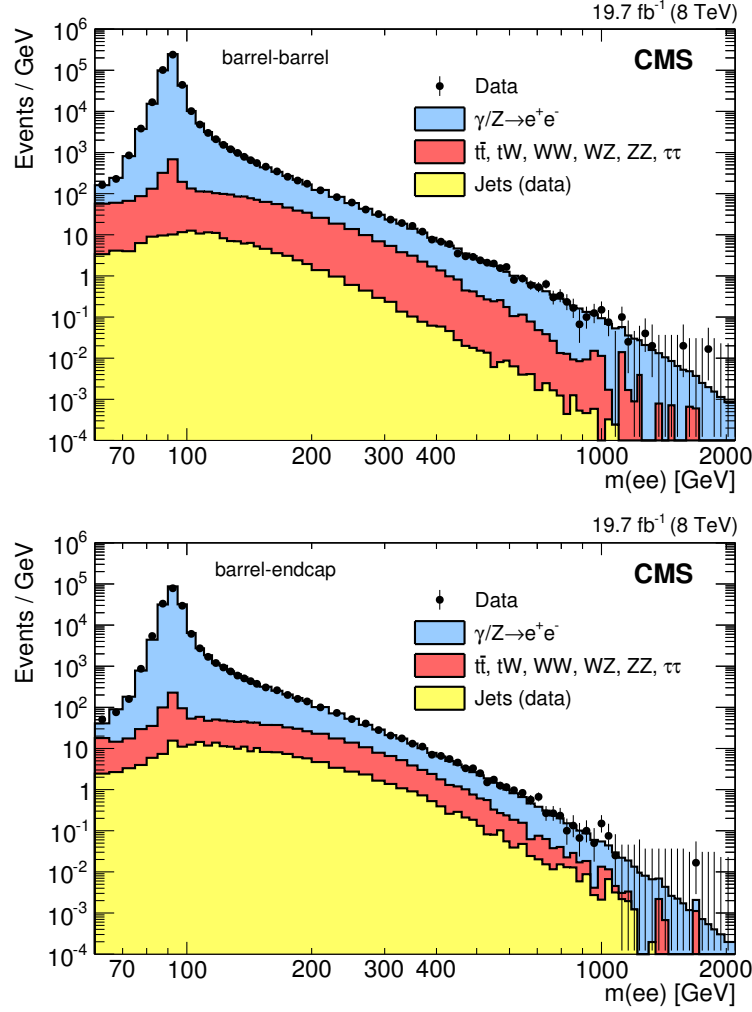


Figure 3. The invariant mass spectrum for ee events separated into barrel-barrel (top) and barrel-endcap (bottom) categories. The points with error bars represent the data. The histograms represent the expectations from SM processes: Z/γ^* , $t\bar{t}$, and other sources of prompt leptons (tW , diboson production, $Z/\gamma^* \rightarrow \tau^+\tau^-$), as well as the multijet backgrounds. Multijet backgrounds contain at least one jet that has been misreconstructed as an electron. The simulated backgrounds are normalized to the data using events in the region of $60 < m_{ee} < 120$ GeV.

correspond to a mass range of $\pm 5\% \sqrt{s}$ [43] about the Z' on-shell mass and a mass range of ± 30 GeV about the Z peak. This Z' mass window is designed to ensure the results are as model independent as possible, allowing for straightforward reinterpretation of the limits derived in this paper in the context of models not specifically addressed. The window chosen reduces model-dependent effects such as $Z/\gamma^*/Z'$ interference and low mass tails due to higher parton luminosities at lower values of \sqrt{s} .

The statistical procedure presented in this section is identical to that used in refs. [16, 44], with the exception that barrel-barrel and barrel-endcap electron events are now treated as separate channels. This is because the signal-to-background ratios and

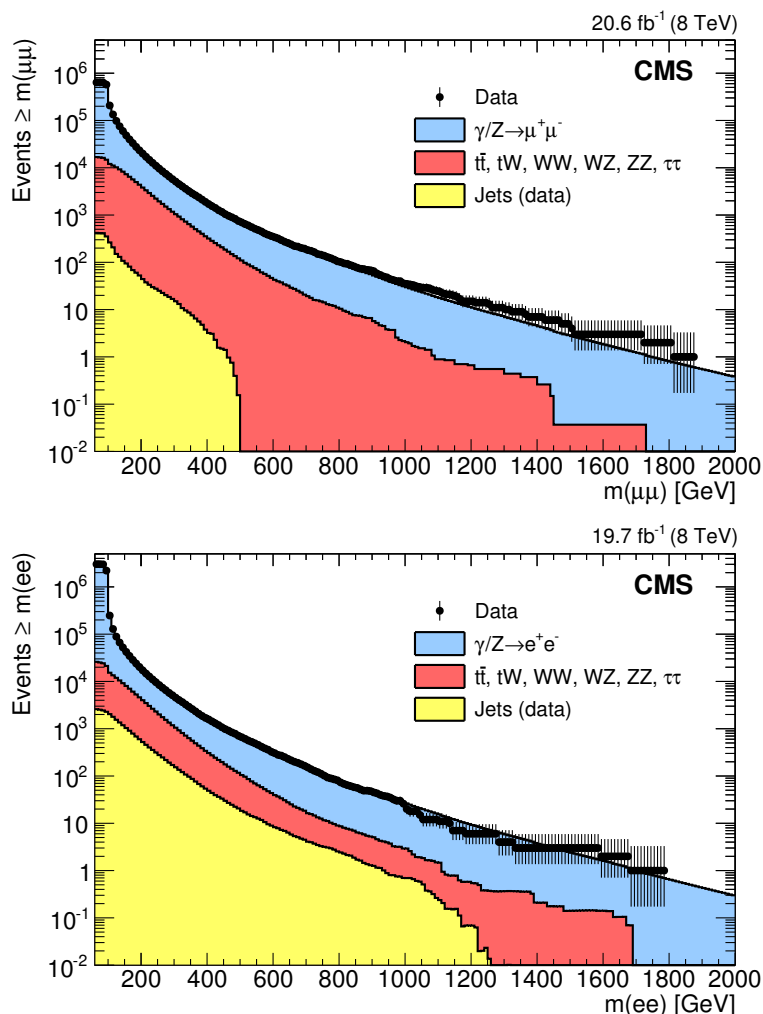


Figure 4. The cumulative distribution, where all events above the specified mass on the x axis are summed, of the invariant mass spectrum of $\mu^+\mu^-$ (top) and ee (bottom) events. The points with error bars represent the data; the histograms represent the expectations from standard model processes. The simulated backgrounds are normalized to the number of events in the data in the region of $60 < m_{\ell\ell} < 120$ GeV, with the dimuon channel using events collected with a prescaled lower-threshold trigger.

mass resolutions differ in the barrel and endcap regions, and the mass limits are sensitive to these quantities. As an example, at 500 GeV, the mass resolution in the barrel-barrel channel is 1.2% while it is 1.9% in the barrel-endcap channel. These resolutions remain fairly constant above 500 GeV. At high masses where there is little background, the separation into the two channels does not result in significantly improved limits. The dimuon mass resolution is similar in all regions and hence no differentiation into separate regions is used. The resolution varies with mass, ranging from approximately 3% at 500 GeV to 9% at 3 TeV. In the case of electrons, the mass resolution is dominated by the energy resolution, and for muons by the momentum resolution. A key feature of the limit-setting

	α (GeV $^{-1}$)	β (GeV $^{-2}$)	κ
$\mu^+\mu^-$	-2.29×10^{-3}	3.32×10^{-8}	-3.65
ee barrel-barrel	-1.16×10^{-3}	-2.02×10^{-7}	-3.97
ee barrel-endcap	-3.79×10^{-3}	1.86×10^{-7}	-3.15

Table 4. The parameters α , β and κ in the background function $m^\kappa e^{\alpha m + \beta m^2}$ obtained from a fit to the background simulation, where the mass m is in GeV.

procedure is that it requires no knowledge of the integrated luminosity as the background estimations are normalized to the data in regions where contributions from SM processes are large compared to any potential signal and the limits are set on the ratio of Z' to Z cross sections.

7.2 Resonance search likelihood function

The extended unbinned likelihood function for the invariant mass spectrum consists of a sum of probability density functions (pdf) for the signal and background shapes, where the signal fraction is set to zero for the background-only hypothesis. The signal is parametrized as a convolution of a Breit-Wigner (BW) and a Gaussian resolution function. The BW width is sufficiently small that the detector resolution dominates.

The Poisson mean of the signal yield is $\mu_S = R_\sigma \mu_Z \cdot R_\epsilon$, where R_σ is defined in eq. (7.1) and R_ϵ is the ratio of the selection efficiency times detector acceptance for the Z' decay relative to that of the Z decay. The variable μ_Z is the Poisson mean of the number of $Z \rightarrow \ell\ell$ events. It is estimated by counting the number of events in the Z boson mass region, where the background contamination is predicted to be small ($\approx 0.5\%$ in simulation). The quantities μ_Z and R_ϵ are obtained separately for the dimuon and dielectron channels.

A background pdf f_B is chosen and its shape parameters fixed by fitting to the full SM background estimate in the mass range $200 < m_{\ell\ell} < 3500$ GeV. The functional form used for the background is $m^\kappa e^{\alpha m + \beta m^2}$. This form includes an m^2 term, which previous versions of this analysis [16] did not include. The increasing range of the fit has required this addition to ensure that the background is well described across the entire range. The parameters α , β , and κ , obtained from fitting to the simulation and subsequently used in the limiting setting procedure, are shown in table 4. The simulated background distributions used to obtain the expected limits are normalized to data in the mass regions above 200 GeV in each channel.

Finally, the extended likelihood is:

$$\mathcal{L}(\mathbf{m}|R_\sigma, M, \Gamma, w, \alpha, \beta, \kappa, \mu_B) = \frac{\mu^N e^{-\mu}}{N!} \prod_{i=1}^N \left(\frac{\mu_S(R_\sigma)}{\mu} f_S(m_i|M, \Gamma, w) + \frac{\mu_B}{\mu} f_B(m_i|\alpha, \beta, \kappa) \right), \quad (7.2)$$

where \mathbf{m} denotes the data set in which the observables are the invariant mass values of the lepton pairs, m_i ; N denotes the total number of events observed in the mass window for which the likelihood is evaluated; μ_B denotes the Poisson mean of the total background

yield; and $\mu = \mu_S + \mu_B$ is the mean of the Poisson distribution from which N is an observation. The mass and width of the Breit-Wigner function are denoted by M and Γ , and w denotes the width of the Gaussian resolution function. The signal and background pdf's are denoted by f_S and f_B .

7.3 Non-resonant searches

The ADD and CI searches both use the same methodology and are based on counting events above mass thresholds. In the ADD analysis an optimal minimum mass threshold is chosen to maximize the limit on the parameter Λ_T using expected limits, and a similar procedure is followed in the CI analysis, where the relevant parameter is the energy scale Λ , and both destructive and constructive interference scenarios are considered.

7.4 Non-resonant likelihood function

The probability of observing a number N_{obs} of events is given by the Poisson likelihood

$$\mathcal{P}(N_{\text{obs}}) = \frac{a^{N_{\text{obs}}}}{N_{\text{obs}}!} e^{-a}, \quad (7.3)$$

where a is the assumed Poisson mean. Both the background and a potential signal can contribute to the Poisson mean, a , which can be expressed as

$$a = (\epsilon_s \sigma_s + \epsilon_b \sigma_b) \frac{N_{\text{obs},Z}}{\sigma_Z \epsilon_Z}, \quad (7.4)$$

where σ_s and σ_b are the respective cross sections of the signal and the background, and ϵ_s, ϵ_b are the total efficiencies (including acceptances) for the signal and background, respectively. The expected number of background events is estimated using the number of events in a mass window of ± 30 GeV around the Z peak, as in the resonance analysis. In eq. (7.4) the relevant quantities are indicated by the subscript Z.

7.5 Uncertainties

The sources of uncertainty are the same in all of the interpretations of the observed spectra. However, because the Z' analysis makes use only of the background shape and the ADD and CI analyses are based on counting events, the importance of the uncertainties differs. In general, the uncertainties have little effect on the derived limits, particularly when these limits are set using regions where no events are observed in the data.

The dominant uncertainty in the Z' analysis is from the determination of R_ϵ , the ratio of selection efficiency times detector acceptance for the Z' decay to that of the Z decay. This uncertainty is 3% for the dimuon channel, 4% for the dielectron barrel-barrel channel, and 6% for the barrel-endcap channel. These values reflect the uncertainty in the estimation of the detector acceptance (including the contribution associated with the choice of PDF set) and in the evaluation of the reconstruction efficiency, particularly in the “turn-on” region at low mass.

In the dimuon channel, the effects of the uncertainties in the muon transverse momentum resolution and in the transverse momentum scale at high p_T are evaluated in the

context of both the resonance and non-resonant searches. Different misalignment scenarios where displacements can be incoherent or coherent are considered. The transverse momentum resolution uncertainty has a negligible effect in the resonance analysis and leads to a 5% uncertainty in the predicted background in the non-resonant analyses. Misalignments also lead to a transverse momentum scale uncertainty of 5% per TeV. This has a negligible effect on the resonance analysis, but does dominate the yield uncertainty in the non-resonant search analyses. The uncertainty depends on the lower mass selection threshold $m_{\ell\ell}^{\min}$, and the rapidly falling spectrum leads to an increasing relative uncertainty with the mass threshold. In the ADD analysis $m_{\ell\ell}^{\min} = 1900$ GeV and the uncertainty is 41%. Similarly, in the CI analysis for destructive interference $m_{\ell\ell}^{\min} = 1500$ GeV resulting in an uncertainty of 28% and for constructive interference $m_{\ell\ell}^{\min} = 1200$ GeV, giving a 20% uncertainty.

In both channels the residual background from jets misidentified as leptons is very small, and the uncertainty in this background has a negligible effect on the limit determination.

The PDF uncertainty in the Drell-Yan cross section is evaluated using the PDF4LHC procedure [45, 46]. Cross sections are calculated at next-to-next-to-leading order (NNLO) using FEWZ [47]. The NNLO PDF sets MSTW08 [48], CT10 [49], and NNPDF21 [50] implemented in LHAPDF [51] are used to evaluate the PDF uncertainty as a function of mass. The resulting uncertainties can be parametrized as a quadratic function of mass: $(2.76 + 3.03 \times 10^{-3}m + 2.38 \times 10^{-6}m^2)\%$ for dimuons and $(4.15 + 1.83 \times 10^{-3}m + 2.68 \times 10^{-6}m^2)\%$ for dielectrons, where m is expressed in units of GeV. These uncertainties are included as a function of mass in the limit calculations for all of the analyses. In the non-resonant dielectron analyses the PDF uncertainty dominates.

The POWHEG Monte Carlo simulation includes QCD effects at NLO and electroweak effects at leading order (LO). The FEWZ and HORACE [52–57] programs are used to evaluate the effects of NLO electroweak corrections and the addition of photon induced interactions. The overall correction is found to be approximately constant as a function of the invariant mass, though the size of the photon induced correction is rather sensitive to the PDF set used [58]. In the ADD and CI analysis the correction and its uncertainty, namely 1.0 ± 0.1 , is used for the background prediction. Using FEWZ, a K-factor of 1.024 ± 0.030 is found for QCD NLO to NNLO processes. For the Z' analysis neither of these constant K-factors has any effect on the background uncertainty because the function used to parametrize the background is normalized to the data.

Common systematic uncertainties are taken to be fully correlated in the calculation of combined limits.

7.6 Exclusion limits

A Bayesian limit setting procedure is used for all interpretations of the observed mass spectra. A positive, flat prior is used for the signal cross section as described in refs. [16, 44] and log-normal priors for the systematic uncertainties. The Markov Chain Monte Carlo approach is used for integration.

A prior flat in the signal cross section σ_s yields excellent frequentist coverage properties. Previous searches [14, 28] presented results with prior functions effectively flat in $1/\sqrt{\sigma_s}$, in search regions where interference is negligible for the ADD and CI models [24, 27]. Such priors can exclude a larger M_S (Λ_T) range, however, they are known to have a frequentist coverage of less than 90% for a 95% Bayesian confidence interval in non-resonant searches.

In the Z' search analysis, only events in a window of ± 6 times the mass resolution are considered in the limit setting procedure. To ensure the background is properly constrained, the lower edge of the window is adjusted so that there are at least 400 events in the mass window. The observed limits have been found to be robust and do not significantly change for reasonable variations in the limit setting procedure, such as modifications in the window for accepting events in the likelihood and changes in the background normalization and shape.

Figure 5 shows the observed and expected upper limits on the ratio R_σ of the production cross section times branching fraction of a Z' boson relative to that for a Z boson, for the dimuon and dielectron channels. Figure 6 shows the upper limits for the combined dimuon and dielectron channels for the two spin hypotheses. The figures also show the predicted ratios of cross section times branching fraction for Z'_{SSM} and Z'_ψ production; together with those for G_{KK} production, with the dimensionless graviton coupling to SM fields $k/\overline{M}_{\text{Pl}} = 0.05, 0.01$, and 0.1 . The LO cross section predictions for Z'_{SSM} and Z'_ψ from PYTHIA using the CTEQ6.1 PDF set [59] are corrected by a mass-dependent K-factor obtained using ZWPRODP [60–62], to account for the NNLO QCD contributions. The calculated Z' cross sections include generated dileptons with masses only within $\pm 5\%\sqrt{s}$ of the nominal resonance mass, to enhance sensitivity to a narrow-width resonance [43]. The NNLO prediction used for the Z/γ^* production cross section in the mass window of 60 to 120 GeV is 1.117 nb, which was calculated using FEWZ [47]. The theoretical uncertainty is expected to be 4%, based on 7 TeV studies where factorization and renormalization scales were varied and an uncertainty from PDFs included. No uncertainties in cross sections for the various theoretical Z' models are included when determining the limits.

For the dimuon channel, the 95% CL lower limit on the mass of a Z' resonance is 2.73 (2.39) TeV for Z'_{SSM} (Z'_ψ) and for the dielectron channel it is 2.67 (2.34) TeV for Z'_{SSM} (Z'_ψ). For the combined dimuon and dielectron channels, the 95% CL lower limit on the mass of a Z' resonance is 2.90 (2.57) TeV. Randall-Sundrum Kaluza-Klein gravitons are excluded below 2.56, 2.12, and 1.13 TeV for couplings of 0.10, 0.05, and 0.01 in the dimuon channel and similarly 2.50, 2.13, and 1.25 TeV in the dielectron channel. The combined limits are 2.73, 2.35, and 1.27 TeV. The only limit that differs from the expected value is that for the Randall-Sundrum Kaluza-Klein graviton with a coupling of 0.01, where the expectation is 1.38 TeV. The limits quoted above are a commonly used set of benchmarks. However, the model-independent method used to derive these limits enables them to be reinterpreted in a straightforward way in the context of any model that is characterized by a narrow spin-1 or spin-2 resonance. The discussion that follows illustrates the versatility of these results.

The cross section for charged lepton-pair production via a Z' vector boson can, in the narrow-width approximation (NWA), be expressed in terms of the quantity $c_u w_u + c_d w_d$ [60, 63]. The parameters c_u and c_d contain information from the model-dependent

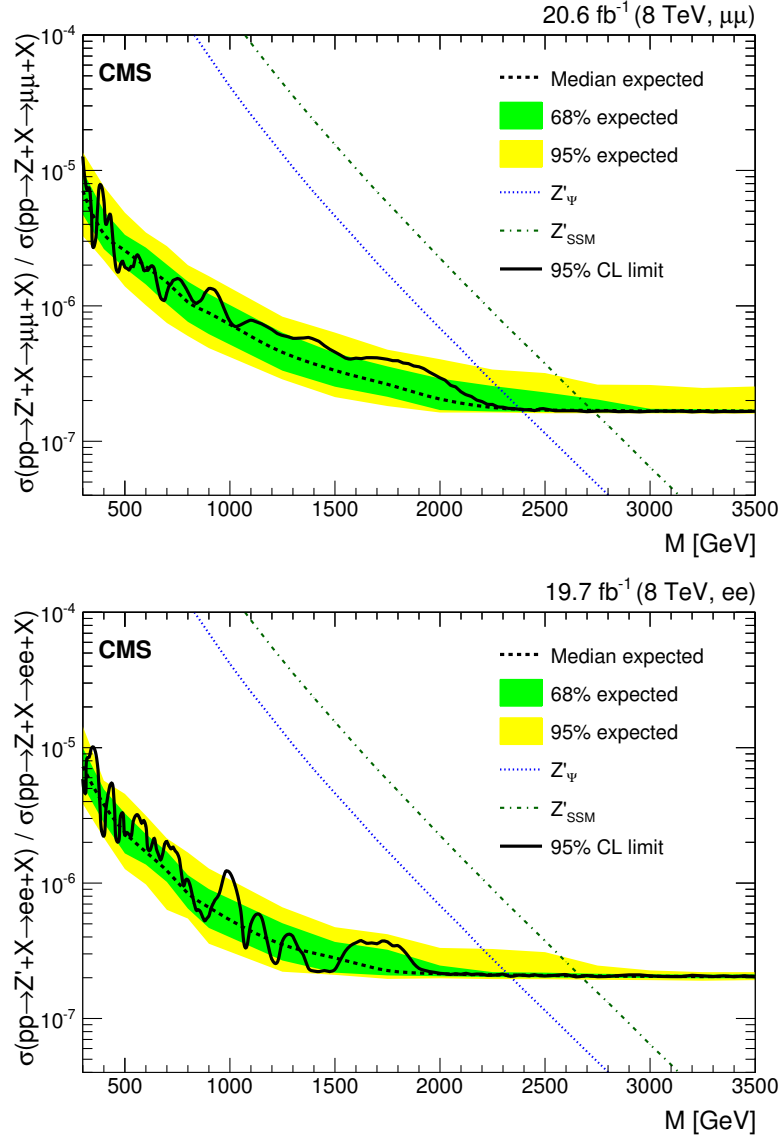


Figure 5. Upper limits as a function of the resonance mass M on the ratio of the product of production cross section and branching fraction into lepton pairs for a spin-1 resonance relative to that of Z bosons. The limits are shown for dimuon (top) and dielectron (bottom) final states. The shaded bands correspond to the 68% and 95% quantiles for the expected limits. Theoretical predictions for spin-1 resonances, Z'_{SSM} and Z'_{ψ} , are shown for comparison.

Z' couplings to fermions in the annihilation of charge $2/3$ and charge $-1/3$ quarks; w_u and w_d contain the information about PDFs for the respective annihilation at a given Z' mass. The translation of the experimental limits into the (c_u, c_d) plane has been studied in the context both of the NWA and taking finite widths into account. The procedures have been shown to give the same results [60]. A further study including the effects of interference [43] has demonstrated that with an appropriate choice of the invariant mass window within which the cross section is calculated, this approach can still be used.

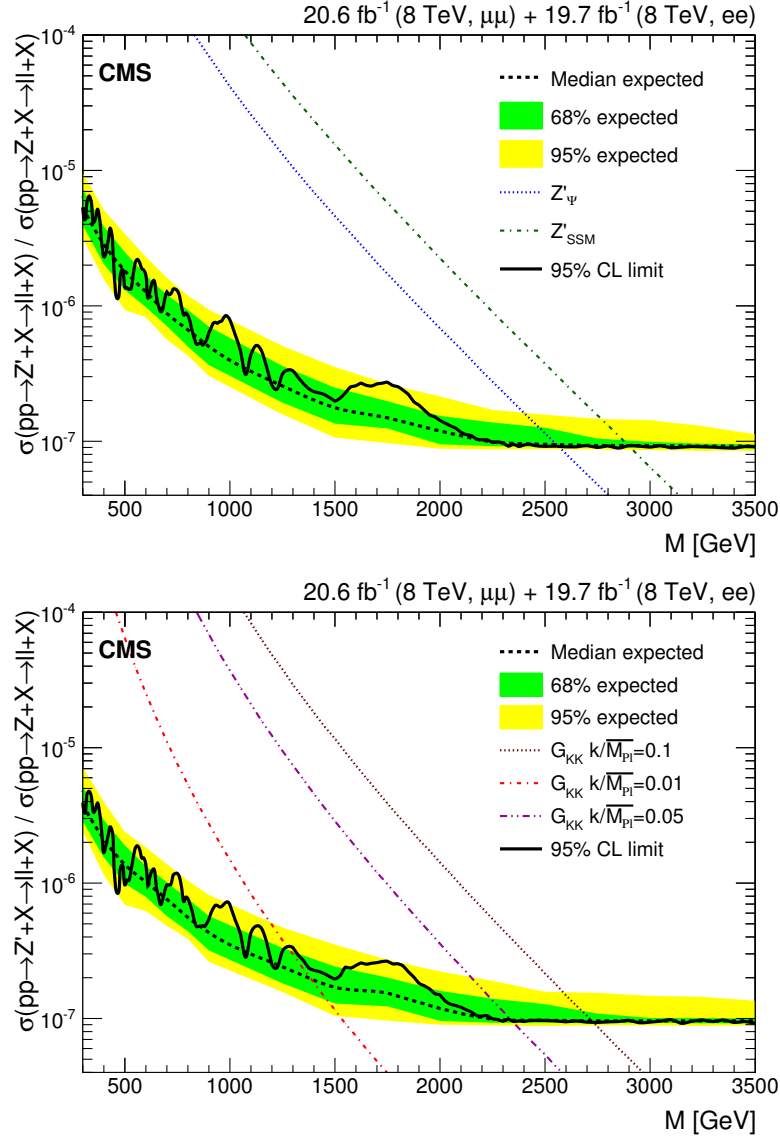


Figure 6. Upper limits as a function of the resonance mass M on the ratio of the product of cross section and branching fraction into lepton pairs relative to that of Z bosons, for final-state spins of 1 (top) and 2 (bottom). The shaded bands correspond to the 68% and 95% quantiles for the expected limits. Theoretical predictions for spin-1 resonances, Z'_{SSM} and Z'_ψ , and spin-2 RS gravitons are shown for comparison.

In figure 7 the limits on the Z' mass are shown as lines in the (c_d, c_u) plane intersected by curves showing (c_d, c_u) as a function of a mixing parameter for various models. In this plane, the thin solid lines labelled by mass are contours of cross section with constant $c_u + (w_d/w_u)c_d$, where w_d/w_u is in the range 0.5–0.6 for the results relevant here. In ref. [60] a number of classes of models were defined, which are illustrated here in figure 7. The Generalized Sequential Model (GSM) class, where the generators of $U(1)_{T_{3L}}$ and $U(1)_Q$ gauge groups [60] mix with mixing angle α , includes the SM-like Z' boson where the

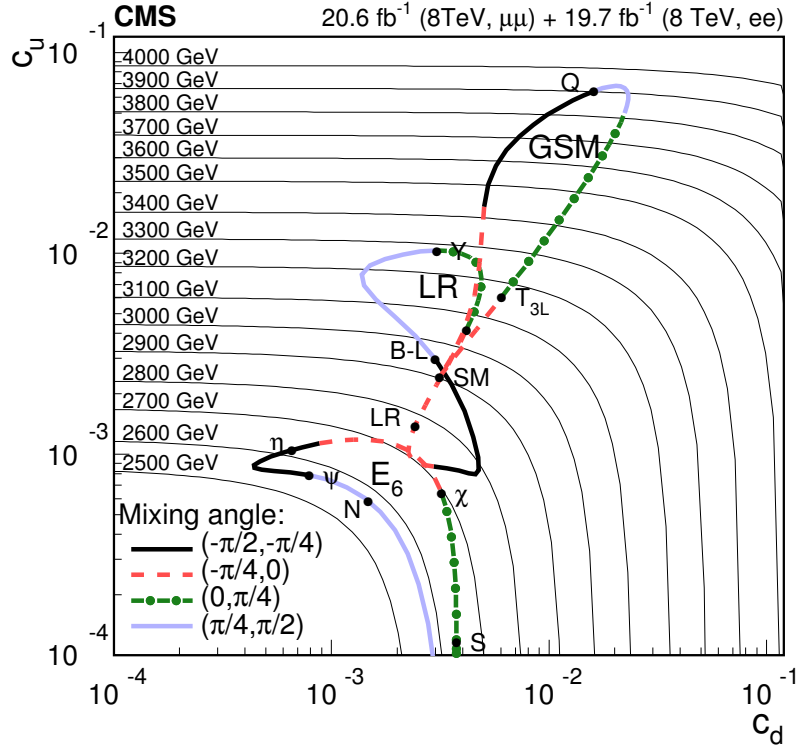


Figure 7. The combined limit on Z' boson mass for dimuon and dielectron channels at 95% CL shown in the (c_u, c_d) plane. The solid thin black lines represent the experimental upper limits on (c_u, c_d) at the masses specified in the figure. The contours representing the GSM, Left-Right, and E_6 model classes are composed of thick line segments. As indicated in the legend, the segment line styles correspond to ranges of the mixing angle.

mixing angle is $\alpha = -0.072\pi$. The angles $\alpha = 0$ and $\alpha = \pi/2$ define the T_{3L} and Q benchmarks, respectively. Also shown are contours for the E_6 model (with χ , ψ , η , S , and N corresponding to angles 0 , 0.5π , -0.29π , 0.13π , and 0.42π) and generalized LR models (with R , $B - L$, LR , and Y corresponding to angles 0 , 0.5π , -0.13π , and 0.25π) [60].

The lower mass thresholds $m_{\ell\ell}^{\min}$ that are used for setting limits in the model of large extra dimensions are chosen to give the largest expected limits. In general, $m_{\ell\ell}^{\min}$ depends on M_{\max} , the scale up to which the theory is valid as described in the Introduction. Thus the value of $m_{\ell\ell}^{\min}$ increases with increasing M_{\max} until a plateau is reached for values of M_{\max} above about 3 TeV. The optimal value of $m_{\ell\ell}^{\min}$ is found to be 1.9 TeV for dimuons and 1.8 TeV for dielectrons.

Limits are set using the dimuon and dielectron mass spectra both separately and combined. Above the respective optimal values of $m_{\ell\ell}^{\min}$ the acceptance is 0.94 for both dimuon and dielectron channels and the cross section limit is found to be 0.19 (0.18) fb in the dimuon (dielectron) channel. Above a mass of 2.0 TeV the cross section for both channels combined is 0.09 fb. The resultant expected and observed limits on the ADD model parameters within the GRW and HLZ conventions are shown in table 5, and the observed limits are shown in figure 8.

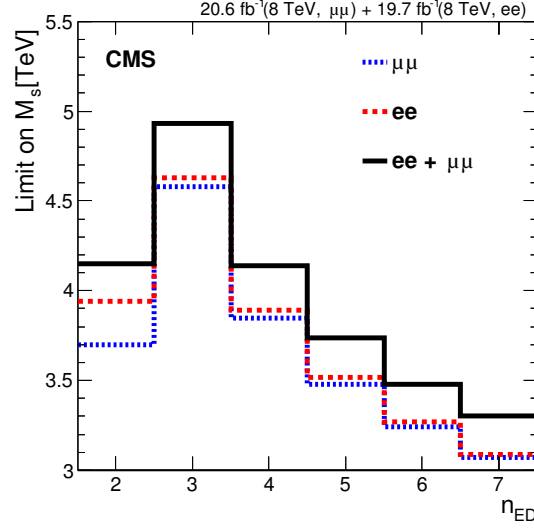


Figure 8. Observed 95% CL limits on M_S for the dimuon (blue), dielectron (red) and combined (black) channel as a function of the number of extra spatial dimensions n_{ED} .

ADD K-factor	Limit	Λ_T (TeV)	M_S (TeV) [HLZ]					
		[GRW]	$n = 2$	$n = 3$	$n = 4$	$n = 5$	$n = 6$	$n = 7$
$\mu\mu, m_{\mu\mu} > 1.9 \text{ TeV}, \sigma_s < 0.19 \text{ fb}$ (0.19 fb expected) at 95% CL								
1.0	expected	3.71	3.46	4.42	3.71	3.36	3.12	2.95
1.3		3.84	3.69	4.57	3.84	3.47	3.23	3.06
1.0	observed	3.72	3.48	4.43	3.72	3.36	3.13	2.96
1.3		3.85	3.70	4.58	3.85	3.48	3.24	3.07
$ee, m_{ee} > 1.8 \text{ TeV}, \sigma_s < 0.18 \text{ fb}$ (0.19 fb expected) at 95% CL								
1.0	expected	3.75	3.73	4.47	3.75	3.39	3.16	2.99
1.3		3.88	3.91	4.61	3.88	3.50	3.26	3.08
1.0	observed	3.77	3.75	4.48	3.77	3.40	3.17	3.00
1.3		3.89	3.94	4.63	3.89	3.52	3.27	3.09
$\mu\mu$ and $ee, m_{\ell\ell} > 2.0 \text{ TeV}, \sigma_s < 0.09 \text{ fb}$ (0.10 fb expected) at 95% CL								
1.0	expected	3.99	3.88	4.74	3.99	3.60	3.35	3.17
1.3		4.13	4.13	4.91	4.13	3.73	3.47	3.28
1.0	observed	4.00	3.90	4.75	4.00	3.61	3.36	3.18
1.3		4.14	4.15	4.93	4.14	3.74	3.48	3.30

Table 5. Observed and expected 95% CL lower limits for the ADD model in the dilepton channels and the combination at 95% CL within GRW and HLZ conventions for truncation at $M_{\text{max}} = M_S$ [HLZ] or $M_{\text{max}} = \Lambda_T$ [GRW].

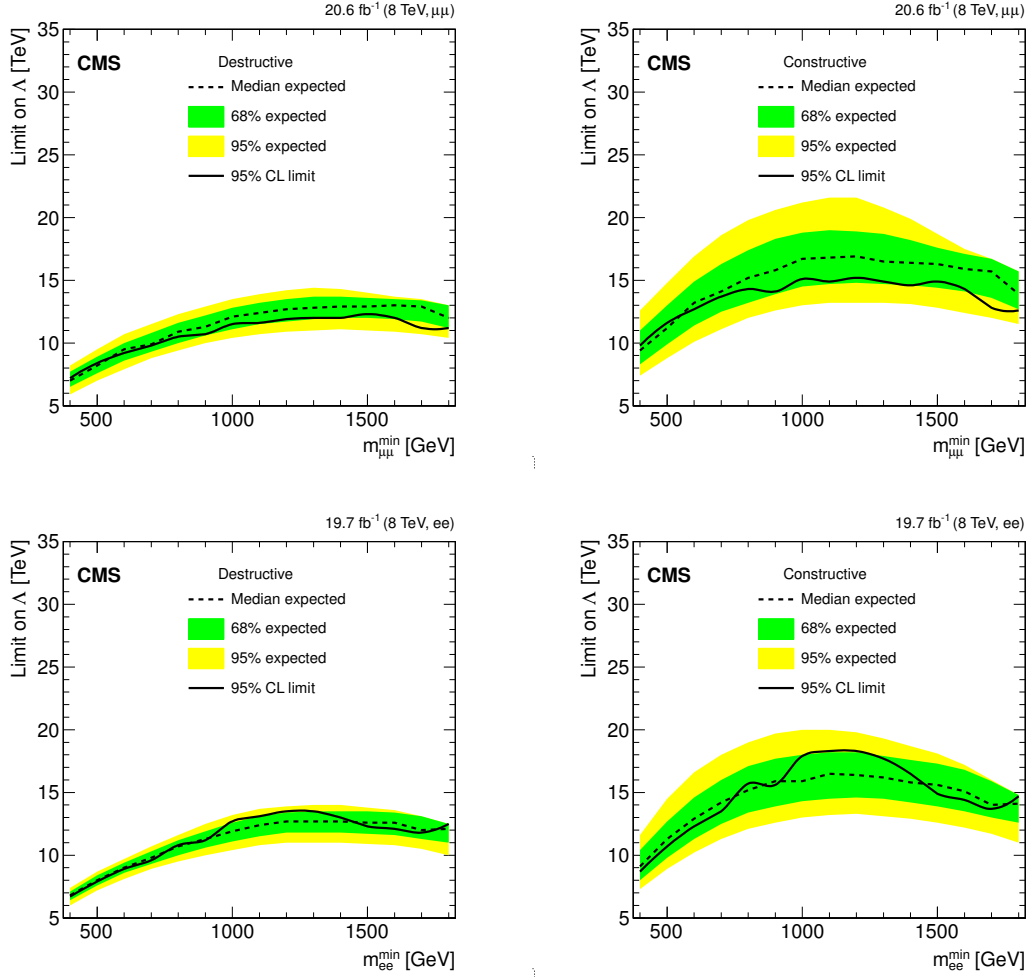


Figure 9. Observed and expected 95% CL limits on Λ : (top) for the dimuon channel as a function of $m_{\mu\mu}^{\min}$ for (left) destructive interference and (right) constructive interference; (bottom) for the dielectron channel as a function of m_{ee}^{\min} for (left) destructive interference and (right) constructive interference.

In order to interpret the observed mass spectra in the context of the contact interaction left-left isoscalar model described in the Introduction, a similar procedure is followed. In this instance there are two cases to consider, namely, where the interference is positive or negative. In each of these cases the expected limits as a function of a minimum mass $m_{\ell\ell}^{\min}$ are found. The value of $m_{\ell\ell}^{\min}$ where the expected limit is a maximum in the dimuon (dielectron) channel is found to be 1500 (1300) GeV for destructive interference and 1200 (1100) GeV for constructive interference. For these values of $m_{\ell\ell}^{\min}$ the observed (expected) limits on Λ for destructive and constructive interference respectively are: 12.0 (13.0) TeV and 15.2 (16.9) TeV for dimuons; and 13.5 (12.7) TeV and 18.3 (16.5) TeV for dielectrons. The observed limits lie almost entirely within 1σ of the expected value, as shown in figure 9.

Under the assumption that the contact interaction with quarks is independent of lepton flavour, the dimuon and dielectron channels can be combined by summing the yields in the two channels. Uncertainties are added in quadrature, taking into account highly correlated sources such as the PDF variations. The observed (expected) limits for this combination are 13.1 (14.1) TeV for destructive interference and 16.9 (17.1) TeV for constructive interference.

8 Summary

A search has been performed, using proton-proton collision data collected at $\sqrt{s} = 8$ TeV, for evidence of physics beyond the standard model in dilepton mass spectra. Data samples correspond to integrated luminosities of 20.6 and 19.7 fb⁻¹ for the dimuon and dielectron channels, respectively. The spectra have been found to be consistent with expectations from the standard model and 95% confidence level limits have been set in the context of various possible new physics models.

In the search for evidence of a narrow resonance, limits have been set on the product of the cross section and branching fraction for new boson production relative to the standard model Z boson production. Mass limits have been set on neutral gauge bosons as follows: a Z' with standard-model-like couplings has been excluded below 2.90 TeV and the superstring-inspired Z'_ψ below 2.57 TeV; Randall-Sundrum Kaluza-Klein gravitons are excluded below 2.73, 2.35, and 1.27 TeV for couplings of 0.10, 0.05, and 0.01, respectively. A notable feature of the resonance analysis is that the limits may be reinterpreted in any model predicting a resonance structure. To enable this, the limits have been calculated in a model-independent way, and the spin-dependent acceptance times efficiency as a function of mass has been provided.

In the search for non-resonant deviations from standard model expectations, limits have been set on the parameters within models of extra dimensions and contact interactions. Within the Arkani-Hamed-Dimopoulos-Dvali model, lower limits have been set on M_S, which characterizes the scale for the onset of quantum gravity. These lower limits range from 4.9 to 3.3 TeV for 3 to 7 additional spatial dimensions. Within the context of the left-left isoscalar contact interaction model, lower limits have been set on the energy scale parameter Λ. For dimuons, the 95% confidence level limit is 12.0 (15.2) TeV for destructive (constructive) interference. Similarly, for dielectrons the limit is 13.5 (18.3) TeV for destructive (constructive) interference. The cross section limits provided along with the dimuon and dielectron acceptances for the ADD model considered may be used to reinterpret these results in the context of other models resulting in non-resonant deviations from SM expectations.

Acknowledgments

We congratulate our colleagues in the CERN accelerator departments for the excellent performance of the LHC and thank the technical and administrative staffs at CERN and at other CMS institutes for their contributions to the success of the CMS effort. In addition, we gratefully acknowledge the computing centres and personnel of the Worldwide

LHC Computing Grid for delivering so effectively the computing infrastructure essential to our analyses. Finally, we acknowledge the enduring support for the construction and operation of the LHC and the CMS detector provided by the following funding agencies: the Austrian Federal Ministry of Science, Research and Economy and the Austrian Science Fund; the Belgian Fonds de la Recherche Scientifique, and Fonds voor Wetenschappelijk Onderzoek; the Brazilian Funding Agencies (CNPq, CAPES, FAPERJ, and FAPESP); the Bulgarian Ministry of Education and Science; CERN; the Chinese Academy of Sciences, Ministry of Science and Technology, and National Natural Science Foundation of China; the Colombian Funding Agency (COLCIENCIAS); the Croatian Ministry of Science, Education and Sport, and the Croatian Science Foundation; the Research Promotion Foundation, Cyprus; the Ministry of Education and Research, Estonian Research Council via IUT23-4 and IUT23-6 and European Regional Development Fund, Estonia; the Academy of Finland, Finnish Ministry of Education and Culture, and Helsinki Institute of Physics; the Institut National de Physique Nucléaire et de Physique des Particules / CNRS, and Commissariat à l'Énergie Atomique et aux Énergies Alternatives / CEA, France; the Bundesministerium für Bildung und Forschung, Deutsche Forschungsgemeinschaft, and Helmholtz-Gemeinschaft Deutscher Forschungszentren, Germany; the General Secretariat for Research and Technology, Greece; the National Scientific Research Foundation, and National Innovation Office, Hungary; the Department of Atomic Energy and the Department of Science and Technology, India; the Institute for Studies in Theoretical Physics and Mathematics, Iran; the Science Foundation, Ireland; the Istituto Nazionale di Fisica Nucleare, Italy; the Ministry of Science, ICT and Future Planning, and National Research Foundation (NRF), Republic of Korea; the Lithuanian Academy of Sciences; the Ministry of Education, and University of Malaya (Malaysia); the Mexican Funding Agencies (CINVESTAV, CONACYT, SEP, and UASLP-FAI); the Ministry of Business, Innovation and Employment, New Zealand; the Pakistan Atomic Energy Commission; the Ministry of Science and Higher Education and the National Science Centre, Poland; the Fundação para a Ciência e a Tecnologia, Portugal; JINR, Dubna; the Ministry of Education and Science of the Russian Federation, the Federal Agency of Atomic Energy of the Russian Federation, Russian Academy of Sciences, and the Russian Foundation for Basic Research; the Ministry of Education, Science and Technological Development of Serbia; the Secretaría de Estado de Investigación, Desarrollo e Innovación and Programa Consolider-Ingenio 2010, Spain; the Swiss Funding Agencies (ETH Board, ETH Zurich, PSI, SNF, UniZH, Canton Zurich, and SER); the Ministry of Science and Technology, Taipei; the Thailand Center of Excellence in Physics, the Institute for the Promotion of Teaching Science and Technology of Thailand, Special Task Force for Activating Research and the National Science and Technology Development Agency of Thailand; the Scientific and Technical Research Council of Turkey, and Turkish Atomic Energy Authority; the National Academy of Sciences of Ukraine, and State Fund for Fundamental Researches, Ukraine; the Science and Technology Facilities Council, UK; the US Department of Energy, and the US National Science Foundation.

Individuals have received support from the Marie-Curie programme and the European Research Council and EPLANET (European Union); the Leventis Foundation; the A. P. Sloan Foundation; the Alexander von Humboldt Foundation; the Belgian Federal

Science Policy Office; the Fonds pour la Formation à la Recherche dans l'Industrie et dans l'Agriculture (FRIA-Belgium); the Agentschap voor Innovatie door Wetenschap en Technologie (IWT-Belgium); the Ministry of Education, Youth and Sports (MEYS) of the Czech Republic; the Council of Science and Industrial Research, India; the HOMING PLUS programme of Foundation for Polish Science, cofinanced from European Union, Regional Development Fund; the Compagnia di San Paolo (Torino); the Consorzio per la Fisica (Trieste); MIUR project 20108T4XTM (Italy); the Thalís and Aristeia programmes cofinanced by EU-ESF and the Greek NSRF; and the National Priorities Research Program by Qatar National Research Fund.

Open Access. This article is distributed under the terms of the Creative Commons Attribution License ([CC-BY 4.0](https://creativecommons.org/licenses/by/4.0/)), which permits any use, distribution and reproduction in any medium, provided the original author(s) and source are credited.

References

- [1] L. Evans and P. Bryant, *LHC machine*, 2008 *JINST* **3** S08001 [[INSPIRE](#)].
- [2] G. Altarelli, B. Mele and M. Ruiz-Altaba, *Searching for new heavy vector bosons in $p\bar{p}$ colliders*, *Z. Phys. C* **45** (1989) 109 [Erratum *ibid.* **C 47** (1990) 676] [[INSPIRE](#)].
- [3] A. Leike, *The phenomenology of extra neutral gauge bosons*, *Phys. Rept.* **317** (1999) 143 [[hep-ph/9805494](#)] [[INSPIRE](#)].
- [4] J.L. Hewett and T.G. Rizzo, *Low-energy phenomenology of superstring inspired E_6 models*, *Phys. Rept.* **183** (1989) 193 [[INSPIRE](#)].
- [5] L. Randall and R. Sundrum, *An alternative to compactification*, *Phys. Rev. Lett.* **83** (1999) 4690 [[hep-th/9906064](#)] [[INSPIRE](#)].
- [6] L. Randall and R. Sundrum, *A large mass hierarchy from a small extra dimension*, *Phys. Rev. Lett.* **83** (1999) 3370 [[hep-ph/9905221](#)] [[INSPIRE](#)].
- [7] N. Arkani-Hamed, S. Dimopoulos and G.R. Dvali, *The hierarchy problem and new dimensions at a millimeter*, *Phys. Lett. B* **429** (1998) 263 [[hep-ph/9803315](#)] [[INSPIRE](#)].
- [8] N. Arkani-Hamed, S. Dimopoulos and G.R. Dvali, *Phenomenology, astrophysics and cosmology of theories with submillimeter dimensions and TeV scale quantum gravity*, *Phys. Rev. D* **59** (1999) 086004 [[hep-ph/9807344](#)] [[INSPIRE](#)].
- [9] E. Eichten, I. Hinchliffe, K.D. Lane and C. Quigg, *Supercollider Physics*, *Rev. Mod. Phys.* **56** (1984) 579 [Addendum *ibid.* **58** (1986) 1065] [[INSPIRE](#)].
- [10] J.L. Hewett, *Indirect collider signals for extra dimensions*, *Phys. Rev. Lett.* **82** (1999) 4765 [[hep-ph/9811356](#)] [[INSPIRE](#)].
- [11] T. Han, J.D. Lykken and R.-J. Zhang, *On Kaluza-Klein states from large extra dimensions*, *Phys. Rev. D* **59** (1999) 105006 [[hep-ph/9811350](#)] [[INSPIRE](#)].
- [12] G.F. Giudice, R. Rattazzi and J.D. Wells, *Quantum gravity and extra dimensions at high-energy colliders*, *Nucl. Phys. B* **544** (1999) 3 [[hep-ph/9811291](#)] [[INSPIRE](#)].
- [13] R. Franceschini, P.P. Giardinò, G.F. Giudice, P. Lodone and A. Strumia, *LHC bounds on large extra dimensions*, *JHEP* **05** (2011) 092 [[arXiv:1101.4919](#)] [[INSPIRE](#)].

- [14] CMS collaboration, *Search for large extra dimensions in dimuon and dielectron events in pp collisions at $\sqrt{s} = 7$ TeV*, *Phys. Lett. B* **711** (2012) 15 [[arXiv:1202.3827](#)] [[INSPIRE](#)].
- [15] E. Eichten, K.D. Lane and M.E. Peskin, *New Tests for Quark and Lepton Substructure*, *Phys. Rev. Lett.* **50** (1983) 811 [[INSPIRE](#)].
- [16] CMS collaboration, *Search for heavy narrow dilepton resonances in pp collisions at $\sqrt{s} = 7$ TeV and $\sqrt{s} = 8$ TeV*, *Phys. Lett. B* **720** (2013) 63 [[arXiv:1212.6175](#)] [[INSPIRE](#)].
- [17] ATLAS collaboration, *Search for high-mass dilepton resonances in pp collisions at $\sqrt{s} = 8$ TeV with the ATLAS detector*, *Phys. Rev. D* **90** (2014) 052005 [[arXiv:1405.4123](#)] [[INSPIRE](#)].
- [18] CDF collaboration, *Search for High-Mass e^+e^- Resonances in $p\bar{p}$ Collisions at $\sqrt{s} = 1.96$ TeV*, *Phys. Rev. Lett.* **102** (2009) 031801 [[arXiv:0810.2059](#)] [[INSPIRE](#)].
- [19] CDF collaboration, *A search for high-mass resonances decaying to dimuons at CDF*, *Phys. Rev. Lett.* **102** (2009) 091805 [[arXiv:0811.0053](#)] [[INSPIRE](#)].
- [20] D0 collaboration, *Search for Randall-Sundrum gravitons in the dielectron and diphoton final states with 5.4 fb^{-1} of data from $p\bar{p}$ collisions at $\sqrt{s} = 1.96$ TeV*, *Phys. Rev. Lett.* **104** (2010) 241802 [[arXiv:1004.1826](#)] [[INSPIRE](#)].
- [21] D0 collaboration, *Search for a heavy neutral gauge boson in the dielectron channel with 5.4 fb^{-1} of $p\bar{p}$ collisions at $\sqrt{s} = 1.96$ TeV*, *Phys. Lett. B* **695** (2011) 88 [[arXiv:1008.2023](#)] [[INSPIRE](#)].
- [22] CDF collaboration, *Search for High Mass Resonances Decaying to Muon Pairs in $\sqrt{s} = 1.96$ TeV $p\bar{p}$ Collisions*, *Phys. Rev. Lett.* **106** (2011) 121801 [[arXiv:1101.4578](#)] [[INSPIRE](#)].
- [23] CDF collaboration, *Search for New Dielectron Resonances and Randall-Sundrum Gravitons at the Collider Detector at Fermilab*, *Phys. Rev. Lett.* **107** (2011) 051801 [[arXiv:1103.4650](#)] [[INSPIRE](#)].
- [24] ATLAS collaboration, *Search for contact interactions and large extra dimensions in the dilepton channel using proton-proton collisions at $\sqrt{s} = 8$ TeV with the ATLAS detector*, *Eur. Phys. J. C* **74** (2014) 3134 [[arXiv:1407.2410](#)] [[INSPIRE](#)].
- [25] ATLAS collaboration, *Search for Contact Interactions in Dimuon Events from pp Collisions at $\sqrt{s} = 7$ TeV with the ATLAS Detector*, *Phys. Rev. D* **84** (2011) 011101 [[arXiv:1104.4398](#)] [[INSPIRE](#)].
- [26] ATLAS collaboration, *Search for contact interactions in dilepton events from pp collisions at $\sqrt{s} = 7$ TeV with the ATLAS detector*, *Phys. Lett. B* **712** (2012) 40 [[arXiv:1112.4462](#)] [[INSPIRE](#)].
- [27] ATLAS collaboration, *Search for contact interactions and large extra dimensions in dilepton events from pp collisions at $\sqrt{s} = 7$ TeV with the ATLAS detector*, *Phys. Rev. D* **87** (2013) 015010 [[arXiv:1211.1150](#)] [[INSPIRE](#)].
- [28] CMS collaboration, *Search for contact interactions in $\mu^+\mu^-$ events in pp collisions at $\sqrt{s} = 7$ TeV*, *Phys. Rev. D* **87** (2013) 032001 [[arXiv:1212.4563](#)] [[INSPIRE](#)].
- [29] CMS collaboration, *The CMS experiment at the CERN LHC*, *2008 JINST* **3** S08004 [[INSPIRE](#)].

- [30] CMS collaboration, *The TriDAS Project Technical Design Report, volume I: The trigger systems*, [CERN-LHCC-2000-038](#); [CMS-TDR-6-1](#) (2000).
- [31] CMS collaboration, *The TriDAS Project Technical Design Report, volume II: Data acquisition and high-level trigger*, [CERN-LHCC-2002-026](#); [CMS-TDR-6](#) (2002).
- [32] CMS collaboration, *Measurements of inclusive W and Z cross sections in pp collisions at $\sqrt{s} = 7$ TeV*, *JHEP* **01** (2011) 080 [[arXiv:1012.2466](#)] [[INSPIRE](#)].
- [33] CMS collaboration, *Performance of CMS muon reconstruction in pp collision events at $\sqrt{s} = 7$ TeV*, *2012 JINST* **7** P10002 [[arXiv:1206.4071](#)] [[INSPIRE](#)].
- [34] CMS collaboration, *Description and performance of track and primary-vertex reconstruction with the CMS tracker*, *2014 JINST* **9** P10009 [[arXiv:1405.6569](#)] [[INSPIRE](#)].
- [35] M. Cacciari and G.P. Salam, *Pileup subtraction using jet areas*, *Phys. Lett. B* **659** (2008) 119 [[arXiv:0707.1378](#)] [[INSPIRE](#)].
- [36] CMS collaboration, *Performance of electron reconstruction and selection with the CMS detector in proton-proton collisions at $\sqrt{s} = 8$ TeV*, [arXiv:1502.02701](#) [[INSPIRE](#)].
- [37] P. Nason, *A new method for combining NLO QCD with shower Monte Carlo algorithms*, *JHEP* **11** (2004) 040 [[hep-ph/0409146](#)] [[INSPIRE](#)].
- [38] S. Frixione, P. Nason and C. Oleari, *Matching NLO QCD computations with Parton Shower simulations: the POWHEG method*, *JHEP* **11** (2007) 070 [[arXiv:0709.2092](#)] [[INSPIRE](#)].
- [39] S. Alioli, P. Nason, C. Oleari and E. Re, *A general framework for implementing NLO calculations in shower Monte Carlo programs: the POWHEG BOX*, *JHEP* **06** (2010) 043 [[arXiv:1002.2581](#)] [[INSPIRE](#)].
- [40] E. Re, *Single-top Wt-channel production matched with parton showers using the POWHEG method*, *Eur. Phys. J. C* **71** (2011) 1547 [[arXiv:1009.2450](#)] [[INSPIRE](#)].
- [41] T. Sjöstrand, S. Mrenna and P.Z. Skands, *PYTHIA 6.4 physics and manual*, *JHEP* **05** (2006) 026 [[hep-ph/0603175](#)] [[INSPIRE](#)].
- [42] J. Alwall et al., *The automated computation of tree-level and next-to-leading order differential cross sections and their matching to parton shower simulations*, *JHEP* **07** (2014) 079 [[arXiv:1405.0301](#)] [[INSPIRE](#)].
- [43] E. Accomando, D. Becciolini, A. Belyaev, S. Moretti and C. Shepherd-Themistocleous, *Z' at the LHC: interference and finite width effects in Drell-Yan*, *JHEP* **10** (2013) 153 [[arXiv:1304.6700](#)] [[INSPIRE](#)].
- [44] CMS collaboration, *Search for resonances in the dilepton mass distribution in pp collisions at $\sqrt{s} = 7$ TeV*, *JHEP* **05** (2011) 093 [[arXiv:1103.0981](#)] [[INSPIRE](#)].
- [45] S. Alekhin et al., *The PDF4LHC Working Group Interim Report*, [arXiv:1101.0536](#) [[INSPIRE](#)].
- [46] M. Botje et al., *The PDF4LHC Working Group Interim Recommendations*, [arXiv:1101.0538](#) [[INSPIRE](#)].
- [47] R. Gavin, Y. Li, F. Petriello and S. Quackenbush, *FEWZ 2.0: A code for hadronic Z production at next-to-next-to-leading order*, *Comput. Phys. Commun.* **182** (2011) 2388 [[arXiv:1011.3540](#)] [[INSPIRE](#)].
- [48] A.D. Martin, W.J. Stirling, R.S. Thorne and G. Watt, *Parton distributions for the LHC*, *Eur. Phys. J. C* **63** (2009) 189 [[arXiv:0901.0002](#)] [[INSPIRE](#)].

- [49] J. Gao et al., *CT10 next-to-next-to-leading order global analysis of QCD*, *Phys. Rev. D* **89** (2014) 033009 [[arXiv:1302.6246](#)] [[INSPIRE](#)].
- [50] NNPDF collaboration, *A first unbiased global NLO determination of parton distributions and their uncertainties*, *Nucl. Phys. B* **838** (2010) 136 [[arXiv:1102.4407](#)].
- [51] M.R. Whalley, D. Bourilkov and R.C. Group, *The Les Houches accord PDFs (LHAPDF) and LHAGLUE*, [hep-ph/0508110](#) [[INSPIRE](#)].
- [52] C.M. Carloni Calame, G. Montagna, O. Nicrosini and A. Vicini, *Precision electroweak calculation of the production of a high transverse-momentum lepton pair at hadron colliders*, *JHEP* **10** (2007) 109 [[arXiv:0710.1722](#)] [[INSPIRE](#)].
- [53] TEV4LHC-TOP and ELECTROWEAK WORKING GROUP collaborations, *Tevatron-for-LHC Report: Top and Electroweak Physics*, [arXiv:0705.3251](#) [[INSPIRE](#)].
- [54] C.M. Carloni Calame, G. Montagna, O. Nicrosini and A. Vicini, *Precision electroweak calculation of the charged current Drell-Yan process*, *JHEP* **12** (2006) 016 [[hep-ph/0609170](#)] [[INSPIRE](#)].
- [55] C. Buttar et al., *Les Houches physics at TeV colliders 2005, standard model and Higgs working group: Summary report*, [hep-ph/0604120](#) [[INSPIRE](#)].
- [56] C.M. Carloni Calame, G. Montagna, O. Nicrosini and M. Treccani, *Multiple photon corrections to the neutral-current Drell-Yan process*, *JHEP* **05** (2005) 019 [[hep-ph/0502218](#)] [[INSPIRE](#)].
- [57] C.M. Carloni Calame, G. Montagna, O. Nicrosini and M. Treccani, *Higher order QED corrections to W boson mass determination at hadron colliders*, *Phys. Rev. D* **69** (2004) 037301 [[hep-ph/0303102](#)] [[INSPIRE](#)].
- [58] NNPDF collaboration, *Parton distributions with QED corrections*, *Nucl. Phys. B* **877** (2013) 290 [[arXiv:1308.0598](#)] [[INSPIRE](#)].
- [59] J. Pumplin et al., *New generation of parton distributions with uncertainties from global QCD analysis*, *JHEP* **07** (2002) 012 [[hep-ph/0201195](#)] [[INSPIRE](#)].
- [60] E. Accomando, A. Belyaev, L. Fedeli, S.F. King and C. Shepherd-Themistocleous, *Z' physics with early LHC data*, *Phys. Rev. D* **83** (2011) 075012 [[arXiv:1010.6058](#)] [[INSPIRE](#)].
- [61] R. Hamberg, W.L. van Neerven and T. Matsuura, *A Complete calculation of the order α_s^2 correction to the Drell-Yan K factor*, *Nucl. Phys. B* **359** (1991) 343 [Erratum *ibid.* **B 644** (2002) 403] [[INSPIRE](#)].
- [62] W.L. van Neerven and E.B. Zijlstra, *The $O(\alpha_s^2)$ corrected Drell-Yan K factor in the DIS and MS scheme*, *Nucl. Phys. B* **382** (1992) 11 [Erratum *ibid.* **B 680** (2004) 513] [[INSPIRE](#)].
- [63] M. Carena, A. Daleo, B.A. Dobrescu and T.M.P. Tait, *Z' gauge bosons at the Tevatron*, *Phys. Rev. D* **70** (2004) 093009 [[hep-ph/0408098](#)] [[INSPIRE](#)].

The CMS collaboration

Yerevan Physics Institute, Yerevan, Armenia

V. Khachatryan, A.M. Sirunyan, A. Tumasyan

Institut für Hochenergiephysik der OeAW, Wien, Austria

W. Adam, T. Bergauer, M. Dragicevic, J. Erö, C. Fabjan¹, M. Friedl, R. Frühwirth¹, V.M. Ghete, C. Hartl, N. Hörmann, J. Hrubec, M. Jeitler¹, W. Kiesenhofer, V. Knünz, M. Krammer¹, I. Krätschmer, D. Liko, I. Mikulec, D. Rabady², B. Rahbaran, H. Rohringer, R. Schöfbeck, J. Strauss, A. Taurok, W. Treberer-Treberspurg, W. Waltenberger, C.-E. Wulz¹

National Centre for Particle and High Energy Physics, Minsk, Belarus

V. Mossolov, N. Shumeiko, J. Suarez Gonzalez

Universiteit Antwerpen, Antwerpen, Belgium

S. Alderweireldt, M. Bansal, S. Bansal, T. Cornelis, E.A. De Wolf, X. Janssen, A. Knutsson, S. Luyckx, S. Ochesanu, R. Rougny, M. Van De Klundert, H. Van Haevermaet, P. Van Mechelen, N. Van Remortel, A. Van Spilbeeck

Vrije Universiteit Brussel, Brussel, Belgium

F. Blekman, S. Blyweert, J. D'Hondt, N. Daci, N. Heracleous, J. Keaveney, S. Lowette, M. Maes, A. Olbrechts, Q. Python, D. Strom, S. Tavernier, W. Van Doninck, P. Van Mulders, G.P. Van Onsem, I. Villella

Université Libre de Bruxelles, Bruxelles, Belgium

C. Caillol, B. Clerbaux, G. De Lentdecker, D. Dobur, L. Favart, A.P.R. Gay, A. Grebenyuk, A. Léonard, A. Mohammadi, L. Pernie², T. Reis, T. Seva, L. Thomas, C. Vander Velde, P. Vanlaer, J. Wang, F. Zenoni

Ghent University, Ghent, Belgium

V. Adler, K. Beernaert, L. Benucci, A. Cimmino, S. Costantini, S. Crucy, S. Dildick, A. Fagot, G. Garcia, J. McCartin, A.A. Ocampo Rios, D. Ryckbosch, S. Salva Diblen, M. Sigamani, N. Strobbe, F. Thyssen, M. Tytgat, E. Yazgan, N. Zaganidis

Université Catholique de Louvain, Louvain-la-Neuve, Belgium

S. Basegmez, C. Beluffi³, G. Bruno, R. Castello, A. Caudron, L. Ceard, G.G. Da Silva, C. Delaere, T. du Pree, D. Favart, L. Forthomme, A. Giammanco⁴, J. Hollar, A. Jafari, P. Jez, M. Komm, V. Lemaitre, C. Nuttens, D. Pagano, L. Perrini, A. Pin, K. Piotrkowski, A. Popov⁵, L. Quertenmont, M. Selvaggi, M. Vidal Marono, J.M. Vizan Garcia

Université de Mons, Mons, Belgium

N. Belyi, T. Caebergs, E. Daubie, G.H. Hammad

Centro Brasileiro de Pesquisas Fisicas, Rio de Janeiro, Brazil

W.L. Aldá Júnior, G.A. Alves, L. Brito, M. Correa Martins Junior, T. Dos Reis Martins, C. Mora Herrera, M.E. Pol

Universidade do Estado do Rio de Janeiro, Rio de Janeiro, Brazil

W. Carvalho, J. Chinellato⁶, A. Custódio, E.M. Da Costa, D. De Jesus Damiao, C. De Oliveira Martins, S. Fonseca De Souza, H. Malbouisson, D. Matos Figueiredo, L. Mundim, H. Nogima, W.L. Prado Da Silva, J. Santaolalla, A. Santoro, A. Sznajder, E.J. Tonelli Manganote⁶, A. Vilela Pereira

Universidade Estadual Paulista ^a, Universidade Federal do ABC ^b, São Paulo, Brazil

C.A. Bernardes^b, S. Dogra^a, T.R. Fernandez Perez Tomei^a, E.M. Gregores^b, P.G. Mercadante^b, S.F. Novaes^a, Sandra S. Padula^a

Institute for Nuclear Research and Nuclear Energy, Sofia, Bulgaria

A. Aleksandrov, V. Genchev², P. Iaydjiev, A. Marinov, S. Piperov, M. Rodozov, S. Stoykova, G. Sultanov, M. Vutova

University of Sofia, Sofia, Bulgaria

A. Dimitrov, I. Glushkov, R. Hadjiiska, V. Kozhuharov, L. Litov, B. Pavlov, P. Petkov

Institute of High Energy Physics, Beijing, China

J.G. Bian, G.M. Chen, H.S. Chen, M. Chen, R. Du, C.H. Jiang, R. Plestina⁷, F. Romeo, J. Tao, Z. Wang

State Key Laboratory of Nuclear Physics and Technology, Peking University, Beijing, China

C. Asawatangtrakuldee, Y. Ban, Q. Li, S. Liu, Y. Mao, S.J. Qian, D. Wang, W. Zou

Universidad de Los Andes, Bogota, Colombia

C. Avila, L.F. Chaparro Sierra, C. Florez, J.P. Gomez, B. Gomez Moreno, J.C. Sanabria

University of Split, Faculty of Electrical Engineering, Mechanical Engineering and Naval Architecture, Split, Croatia

N. Godinovic, D. Lelas, D. Polic, I. Puljak

University of Split, Faculty of Science, Split, Croatia

Z. Antunovic, M. Kovac

Institute Rudjer Boskovic, Zagreb, Croatia

V. Brigljevic, K. Kadija, J. Luetic, D. Mekterovic, L. Sudic

University of Cyprus, Nicosia, Cyprus

A. Attikis, G. Mavromanolakis, J. Mousa, C. Nicolaou, F. Ptochos, P.A. Razis

Charles University, Prague, Czech Republic

M. Bodlak, M. Finger, M. Finger Jr.⁸

Academy of Scientific Research and Technology of the Arab Republic of Egypt, Egyptian Network of High Energy Physics, Cairo, Egypt

Y. Assran⁹, S. Elgammal¹⁰, M.A. Mahmoud¹¹, A. Radi^{12,13}

National Institute of Chemical Physics and Biophysics, Tallinn, Estonia

M. Kadastik, M. Murumaa, M. Raidal, A. Tiko

Department of Physics, University of Helsinki, Helsinki, Finland

P. Eerola, G. Fedi, M. Voutilainen

Helsinki Institute of Physics, Helsinki, Finland

J. Härkönen, V. Karimäki, R. Kinnunen, M.J. Kortelainen, T. Lampén, K. Lassila-Perini, S. Lehti, T. Lindén, P. Luukka, T. Mäenpää, T. Peltola, E. Tuominen, J. Tuominiemi, E. Tuovinen, L. Wendland

Lappeenranta University of Technology, Lappeenranta, Finland

J. Talvitie, T. Tuuva

DSM/IRFU, CEA/Saclay, Gif-sur-Yvette, France

M. Besancon, F. Couderc, M. Dejardin, D. Denegri, B. Fabbro, J.L. Faure, C. Favaro, F. Ferri, S. Ganjour, A. Givernaud, P. Gras, G. Hamel de Monchenault, P. Jarry, E. Locci, J. Malcles, J. Rander, A. Rosowsky, M. Titov

Laboratoire Leprince-Ringuet, Ecole Polytechnique, IN2P3-CNRS, Palaiseau, France

S. Baffioni, F. Beaudette, P. Busson, C. Charlot, T. Dahms, M. Dalchenko, L. Dobrzynski, N. Filipovic, A. Florent, R. Granier de Cassagnac, L. Mastrolorenzo, P. Miné, C. Mironov, I.N. Naranjo, M. Nguyen, C. Ochando, P. Paganini, S. Regnard, R. Salerno, J.B. Sauvan, Y. Sirois, C. Veelken, Y. Yilmaz, A. Zabi

Institut Pluridisciplinaire Hubert Curien, Université de Strasbourg, Université de Haute Alsace Mulhouse, CNRS/IN2P3, Strasbourg, France

J.-L. Agram¹⁴, J. Andrea, A. Aubin, D. Bloch, J.-M. Brom, E.C. Chabert, C. Collard, E. Conte¹⁴, J.-C. Fontaine¹⁴, D. Gelé, U. Goerlach, C. Goetzmann, A.-C. Le Bihan, P. Van Hove

Centre de Calcul de l'Institut National de Physique Nucleaire et de Physique des Particules, CNRS/IN2P3, Villeurbanne, France

S. Gadrat

Université de Lyon, Université Claude Bernard Lyon 1, CNRS-IN2P3, Institut de Physique Nucléaire de Lyon, Villeurbanne, France

S. Beauceron, N. Beaupere, G. Boudoul², E. Bouvier, S. Brochet, C.A. Carrillo Montoya, J. Chasserat, R. Chierici, D. Contardo², P. Depasse, H. El Mamouni, J. Fan, J. Fay, S. Gascon, M. Gouzevitch, B. Ille, T. Kurca, M. Lethuillier, L. Mirabito, S. Perries, J.D. Ruiz Alvarez, D. Sabes, L. Sgandurra, V. Sordini, M. Vander Donckt, P. Verdier, S. Viret, H. Xiao

Institute of High Energy Physics and Informatization, Tbilisi State University, Tbilisi, Georgia

Z. Tsamalaidze⁸

RWTH Aachen University, I. Physikalisches Institut, Aachen, Germany

C. Autermann, S. Beranek, M. Bontenackels, M. Edelhoff, L. Feld, O. Hindrichs, K. Klein, A. Ostapchuk, A. Perieanu, F. Raupach, J. Sammet, S. Schael, H. Weber, B. Wittmer, V. Zhukov⁵

RWTH Aachen University, III. Physikalisches Institut A, Aachen, Germany

M. Ata, M. Brodski, E. Dietz-Laursonn, D. Duchardt, M. Erdmann, R. Fischer, A. Güth, T. Hebbeker, C. Heidemann, K. Hoepfner, D. Klingebiel, S. Knutzen, P. Kreuzer, M. Merschmeyer, A. Meyer, P. Millet, M. Olschewski, K. Padeken, P. Papacz, T. Pook, H. Reithler, S.A. Schmitz, L. Sonnenschein, D. Teyssier, S. Thüer, M. Weber

RWTH Aachen University, III. Physikalisches Institut B, Aachen, Germany

V. Cherepanov, Y. Erdogan, G. Flügge, H. Geenen, M. Geisler, W. Haj Ahmad, A. Heister, F. Hoehle, B. Kargoll, T. Kress, Y. Kuessel, A. Künsken, J. Lingemann², A. Nowack, I.M. Nugent, L. Perchalla, O. Pooth, A. Stahl

Deutsches Elektronen-Synchrotron, Hamburg, Germany

I. Asin, N. Bartosik, J. Behr, W. Behrenhoff, U. Behrens, A.J. Bell, M. Bergholz¹⁵, A. Bethani, K. Borras, A. Burgmeier, A. Cakir, L. Calligaris, A. Campbell, S. Choudhury, F. Costanza, C. Diez Pardos, S. Dooling, T. Dorland, G. Eckerlin, D. Eckstein, T. Eichhorn, G. Flucke, J. Garay Garcia, A. Geiser, P. Gunnellini, J. Hauk, M. Hempel¹⁵, D. Horton, H. Jung, A. Kalogeropoulos, M. Kasemann, P. Katsas, J. Kieseler, C. Kleinwort, D. Krücker, W. Lange, J. Leonard, K. Lipka, A. Lobanov, W. Lohmann¹⁵, B. Lutz, R. Mankel, I. Marfin¹⁵, I.-A. Melzer-Pellmann, A.B. Meyer, G. Mittag, J. Mnich, A. Mussgiller, S. Naumann-Emme, A. Nayak, O. Novgorodova, E. Ntomari, H. Perrey, D. Pitzl, R. Placakyte, A. Raspereza, P.M. Ribeiro Cipriano, B. Roland, E. Ron, M.Ö. Sahin, J. Salfeld-Nebgen, P. Saxena, R. Schmidt¹⁵, T. Schoerner-Sadenius, M. Schröder, C. Seitz, S. Spannagel, A.D.R. Vargas Trevino, R. Walsh, C. Wissing

University of Hamburg, Hamburg, Germany

M. Aldaya Martin, V. Blobel, M. Centis Vignali, A.R. Draeger, J. Erfle, E. Garutti, K. Goebel, M. Görner, J. Haller, M. Hoffmann, R.S. Höing, H. Kirschenmann, R. Klanner, R. Kogler, J. Lange, T. Lapsien, T. Lenz, I. Marchesini, J. Ott, T. Peiffer, N. Pietsch, J. Poehlsen, T. Poehlsen, D. Rathjens, C. Sander, H. Schettler, P. Schleper, E. Schlieckau, A. Schmidt, M. Seidel, V. Sola, H. Stadie, G. Steinbrück, D. Troendle, E. Usai, L. Vanelderden, A. Vanhoefer

Institut für Experimentelle Kernphysik, Karlsruhe, Germany

C. Barth, C. Baus, J. Berger, C. Böser, E. Butz, T. Chwalek, W. De Boer, A. Descroix, A. Dierlamm, M. Feindt, F. Fensch, M. Giffels, F. Hartmann², T. Hauth², U. Husemann, I. Katkov⁵, A. Kornmayer², E. Kuznetsova, P. Lobelle Pardo, M.U. Mozer, Th. Müller, A. Nürnberg, G. Quast, K. Rabbertz, F. Ratnikov, S. Röcker, H.J. Simonis, F.M. Stober, R. Ulrich, J. Wagner-Kuhr, S. Wayand, T. Weiler, R. Wolf

Institute of Nuclear and Particle Physics (INPP), NCSR Demokritos, Aghia Paraskevi, Greece

G. Anagnostou, G. Daskalakis, T. Gerasis, V.A. Giakoumopoulou, A. Kyriakis, D. Loukas, A. Markou, C. Markou, A. Psallidas, I. Topsis-Giotis

University of Athens, Athens, Greece

A. Agapitos, S. Kesisoglou, A. Panagiotou, N. Saoulidou, E. Stiliaris

University of Ioánnina, Ioánnina, Greece

X. Aslanoglou, I. Evangelou, G. Flouris, C. Foudas, P. Kokkas, N. Manthos, I. Papadopoulos, E. Paradas

Wigner Research Centre for Physics, Budapest, Hungary

G. Bencze, C. Hajdu, P. Hidas, D. Horvath¹⁶, F. Sikler, V. Veszpremi, G. Vesztergombi¹⁷, A.J. Zsigmond

Institute of Nuclear Research ATOMKI, Debrecen, Hungary

N. Beni, S. Czellar, J. Karancsi¹⁸, J. Molnar, J. Palinkas, Z. Szillasi

University of Debrecen, Debrecen, Hungary

P. Raics, Z.L. Trocsanyi, B. Ujvari

National Institute of Science Education and Research, Bhubaneswar, India

S.K. Swain

Panjab University, Chandigarh, India

S.B. Beri, V. Bhatnagar, R. Gupta, U.Bhawandeep, A.K. Kalsi, M. Kaur, R. Kumar, M. Mittal, N. Nishu, J.B. Singh

University of Delhi, Delhi, India

Ashok Kumar, Arun Kumar, S. Ahuja, A. Bhardwaj, B.C. Choudhary, A. Kumar, S. Malhotra, M. Naimuddin, K. Ranjan, V. Sharma

Saha Institute of Nuclear Physics, Kolkata, India

S. Banerjee, S. Bhattacharya, K. Chatterjee, S. Dutta, B. Gomber, Sa. Jain, Sh. Jain, R. Khurana, A. Modak, S. Mukherjee, D. Roy, S. Sarkar, M. Sharan

Bhabha Atomic Research Centre, Mumbai, India

A. Abdulsalam, D. Dutta, S. Kailas, V. Kumar, A.K. Mohanty², L.M. Pant, P. Shukla, A. Topkar

Tata Institute of Fundamental Research, Mumbai, India

T. Aziz, S. Banerjee, S. Bhowmik¹⁹, R.M. Chatterjee, R.K. Dewanjee, S. Dugad, S. Ganguly, S. Ghosh, M. Guchait, A. Gurtu²⁰, G. Kole, S. Kumar, M. Maity¹⁹, G. Majumder, K. Mazumdar, G.B. Mohanty, B. Parida, K. Sudhakar, N. Wickramage²¹

Institute for Research in Fundamental Sciences (IPM), Tehran, Iran

H. Bakhshiansohi, H. Behnamian, S.M. Etesami²², A. Fahim²³, R. Goldouzian, M. Khakzad, M. Mohammadi Najafabadi, M. Naseri, S. Paktinat Mehdiabadi, F. Rezaei Hosseinabadi, B. Safarzadeh²⁴, M. Zeinali

University College Dublin, Dublin, Ireland

M. Felcini, M. Grunewald

INFN Sezione di Bari ^a, Università di Bari ^b, Politecnico di Bari ^c, Bari, Italy

M. Abbrescia^{a,b}, L. Barbone^{a,b}, C. Calabria^{a,b}, S.S. Chhibra^{a,b}, A. Colaleo^a, D. Creanza^{a,c}, N. De Filippis^{a,c}, M. De Palma^{a,b}, L. Fiore^a, G. Iaselli^{a,c}, G. Maggi^{a,c}, M. Maggi^a, S. My^{a,c}, S. Nuzzo^{a,b}, A. Pompili^{a,b}, G. Pugliese^{a,c}, R. Radogna^{a,b,2}, G. Selvaggi^{a,b}, A. Sharma, L. Silvestris^{a,2}, R. Venditti^{a,b}, G. Zito^a

INFN Sezione di Bologna ^a, Università di Bologna ^b, Bologna, Italy

G. Abbiendi^a, A.C. Benvenuti^a, D. Bonacorsi^{a,b}, S. Braibant-Giacomelli^{a,b}, L. Brigliadori^{a,b}, R. Campanini^{a,b}, P. Capiluppi^{a,b}, A. Castro^{a,b}, F.R. Cavallo^a, G. Codispoti^{a,b}, M. Cuffiani^{a,b}, G.M. Dallavalle^a, F. Fabbri^a, A. Fanfani^{a,b}, D. Fasanella^{a,b}, P. Giacomelli^a, C. Grandi^a, L. Guiducci^{a,b}, S. Marcellini^a, G. Masetti^a, A. Montanari^a, F.L. Navarria^{a,b}, A. Perrotta^a, F. Primavera^{a,b}, A.M. Rossi^{a,b}, T. Rovelli^{a,b}, G.P. Siroli^{a,b}, N. Tosi^{a,b}, R. Travaglini^{a,b}

INFN Sezione di Catania ^a, Università di Catania ^b, CSFNSM ^c, Catania, Italy

S. Albergo^{a,b}, G. Cappello^a, M. Chiorboli^{a,b}, S. Costa^{a,b}, F. Giordano^{a,c,2}, R. Potenza^{a,b}, A. Tricomi^{a,b}, C. Tuve^{a,b}

INFN Sezione di Firenze ^a, Università di Firenze ^b, Firenze, Italy

G. Barbagli^a, V. Ciulli^{a,b}, C. Civinini^a, R. D'Alessandro^{a,b}, E. Focardi^{a,b}, E. Gallo^a, S. Gonzi^{a,b}, V. Gori^{a,b,2}, P. Lenzi^{a,b}, M. Meschini^a, S. Paoletti^a, G. Sguazzoni^a, A. Tropiano^{a,b}

INFN Laboratori Nazionali di Frascati, Frascati, Italy

L. Benussi, S. Bianco, F. Fabbri, D. Piccolo

INFN Sezione di Genova ^a, Università di Genova ^b, Genova, Italy

R. Ferretti^{a,b}, F. Ferro^a, M. Lo Vetere^{a,b}, E. Robutti^a, S. Tosi^{a,b}

INFN Sezione di Milano-Bicocca ^a, Università di Milano-Bicocca ^b, Milano, Italy

M.E. Dinardo^{a,b}, S. Fiorendi^{a,b,2}, S. Gennai^{a,2}, R. Gerosa^{a,b,2}, A. Ghezzi^{a,b}, P. Govoni^{a,b}, M.T. Lucchini^{a,b,2}, S. Malvezzi^a, R.A. Manzoni^{a,b}, A. Martelli^{a,b}, B. Marzocchi^{a,b}, D. Menasce^a, L. Moroni^a, M. Paganoni^{a,b}, D. Pedrini^a, S. Ragazzi^{a,b}, N. Redaelli^a, T. Tabarelli de Fatis^{a,b}

INFN Sezione di Napoli ^a, Università di Napoli 'Federico II' ^b, Università della Basilicata (Potenza) ^c, Università G. Marconi (Roma) ^d, Napoli, Italy

S. Buontempo^a, N. Cavallo^{a,c}, S. Di Guida^{a,d,2}, F. Fabozzi^{a,c}, A.O.M. Iorio^{a,b}, L. Lista^a, S. Meola^{a,d,2}, M. Merola^a, P. Paolucci^{a,2}

INFN Sezione di Padova ^a, Università di Padova ^b, Università di Trento (Trento) ^c, Padova, Italy

P. Azzi^a, N. Bacchetta^a, D. Bisello^{a,b}, A. Branca^{a,b}, R. Carlin^{a,b}, P. Checchia^a, M. Dall'Osso^{a,b}, T. Dorigo^a, U. Dosselli^a, M. Galanti^{a,b}, F. Gasparini^{a,b}, U. Gasparini^{a,b},

P. Giubilato^{a,b}, A. Gozzelino^a, K. Kanishchev^{a,c}, S. Lacaprarà^a, M. Margoni^{a,b}, A.T. Meneguzzo^{a,b}, J. Pazzini^{a,b}, N. Pozzobon^{a,b}, P. Ronchese^{a,b}, F. Simonetto^{a,b}, E. Torassa^a, M. Tosi^{a,b}, P. Zotto^{a,b}, A. Zucchetta^{a,b}, G. Zumerle^{a,b}

INFN Sezione di Pavia ^a, Università di Pavia ^b, Pavia, Italy

M. Gabusi^{a,b}, S.P. Ratti^{a,b}, V. Re^a, C. Riccardi^{a,b}, P. Salvini^a, P. Vitulo^{a,b}

INFN Sezione di Perugia ^a, Università di Perugia ^b, Perugia, Italy

M. Biasini^{a,b}, G.M. Bilei^a, D. Ciangottini^{a,b}, L. Fanò^{a,b}, P. Lariccia^{a,b}, G. Mantovani^{a,b}, M. Menichelli^a, A. Saha^a, A. Santocchia^{a,b}, A. Spiezia^{a,b,2}

INFN Sezione di Pisa ^a, Università di Pisa ^b, Scuola Normale Superiore di Pisa ^c, Pisa, Italy

K. Androsov^{a,25}, P. Azzurri^a, G. Bagliesi^a, J. Bernardini^a, T. Boccali^a, G. Broccolo^{a,c}, R. Castaldi^a, M.A. Ciocci^{a,25}, R. Dell’Orso^a, S. Donato^{a,c}, F. Fiori^{a,c}, L. Foà^{a,c}, A. Giassi^a, M.T. Grippo^{a,25}, F. Ligabue^{a,c}, T. Lomtadze^a, L. Martini^{a,b}, A. Messineo^{a,b}, C.S. Moon^{a,26}, F. Palla^{a,2}, A. Rizzi^{a,b}, A. Savoy-Navarro^{a,27}, A.T. Serban^a, P. Spagnolo^a, P. Squillacioti^{a,25}, R. Tenchini^a, G. Tonelli^{a,b}, A. Venturi^a, P.G. Verдини^a, C. Vernieri^{a,c,2}

INFN Sezione di Roma ^a, Università di Roma ^b, Roma, Italy

L. Barone^{a,b}, F. Cavallari^a, G. D’imperio^{a,b}, D. Del Re^{a,b}, M. Diemoz^a, M. Grassi^{a,b}, C. Jorda^a, E. Longo^{a,b}, F. Margaroli^{a,b}, P. Meridiani^a, F. Micheli^{a,b,2}, S. Nourbakhsh^{a,b}, G. Organtini^{a,b}, R. Paramatti^a, S. Rahatlou^{a,b}, C. Rovelli^a, F. Santanastasio^{a,b}, L. Soffi^{a,b,2}, P. Traczyk^{a,b}

INFN Sezione di Torino ^a, Università di Torino ^b, Università del Piemonte Orientale (Novara) ^c, Torino, Italy

N. Amapane^{a,b}, R. Arcidiacono^{a,c}, S. Argiro^{a,b}, M. Arneodo^{a,c}, R. Bellan^{a,b}, C. Biino^a, N. Cartiglia^a, S. Casasso^{a,b,2}, M. Costa^{a,b}, A. Degano^{a,b}, N. Demaria^a, L. Finco^{a,b}, C. Mariotti^a, S. Maselli^a, E. Migliore^{a,b}, V. Monaco^{a,b}, M. Musich^a, M.M. Obertino^{a,c,2}, G. Ortona^{a,b}, L. Pacher^{a,b}, N. Pastrone^a, M. Pelliccioni^a, G.L. Pinna Angioni^{a,b}, A. Potenza^{a,b}, A. Romero^{a,b}, M. Ruspa^{a,c}, R. Sacchi^{a,b}, A. Solano^{a,b}, A. Staiano^a, U. Tamponi^a

INFN Sezione di Trieste ^a, Università di Trieste ^b, Trieste, Italy

S. Belforte^a, V. Candelise^{a,b}, M. Casarsa^a, F. Cossutti^a, G. Della Ricca^{a,b}, B. Gobbo^a, C. La Licata^{a,b}, M. Marone^{a,b}, A. Schizzi^{a,b}, T. Umer^{a,b}, A. Zanetti^a

Kangwon National University, Chunchon, Korea

S. Chang, A. Kropivnitskaya, S.K. Nam

Kyungpook National University, Daegu, Korea

D.H. Kim, G.N. Kim, M.S. Kim, D.J. Kong, S. Lee, Y.D. Oh, H. Park, A. Sakharov, D.C. Son

Chonbuk National University, Jeonju, Korea

T.J. Kim

Chonnam National University, Institute for Universe and Elementary Particles, Kwangju, Korea

J.Y. Kim, S. Song

Korea University, Seoul, Korea

S. Choi, D. Gyun, B. Hong, M. Jo, H. Kim, Y. Kim, B. Lee, K.S. Lee, S.K. Park, Y. Roh

Seoul National University, Seoul, Korea

H.D. Yoo

University of Seoul, Seoul, Korea

M. Choi, J.H. Kim, I.C. Park, G. Ryu, M.S. Ryu

Sungkyunkwan University, Suwon, Korea

Y. Choi, Y.K. Choi, J. Goh, D. Kim, E. Kwon, J. Lee, H. Seo, I. Yu

Vilnius University, Vilnius, Lithuania

A. Juodagalvis

National Centre for Particle Physics, Universiti Malaya, Kuala Lumpur, Malaysia

J.R. Komaragiri, M.A.B. Md Ali

Centro de Investigacion y de Estudios Avanzados del IPN, Mexico City, Mexico

H. Castilla-Valdez, E. De La Cruz-Burelo, I. Heredia-de La Cruz²⁸, A. Hernandez-Almada, R. Lopez-Fernandez, A. Sanchez-Hernandez

Universidad Iberoamericana, Mexico City, Mexico

S. Carrillo Moreno, F. Vazquez Valencia

Benemerita Universidad Autonoma de Puebla, Puebla, Mexico

I. Pedraza, H.A. Salazar Ibarguen

Universidad Autónoma de San Luis Potosí, San Luis Potosí, Mexico

E. Casimiro Linares, A. Morelos Pineda

University of Auckland, Auckland, New Zealand

D. Krofcheck

University of Canterbury, Christchurch, New Zealand

P.H. Butler, S. Reucroft

National Centre for Physics, Quaid-I-Azam University, Islamabad, Pakistan

A. Ahmad, M. Ahmad, Q. Hassan, H.R. Hoorani, S. Khalid, W.A. Khan, T. Khurshid, M.A. Shah, M. Shoaib

National Centre for Nuclear Research, Swierk, Poland

H. Bialkowska, M. Bluj, B. Boimska, T. Frueboes, M. Górski, M. Kazana, K. Nawrocki, K. Romanowska-Rybinska, M. Szleper, P. Zalewski

Institute of Experimental Physics, Faculty of Physics, University of Warsaw, Warsaw, Poland

G. Brona, K. Bunkowski, M. Cwiok, W. Dominik, K. Doroba, A. Kalinowski, M. Konecki, J. Krolikowski, M. Misiura, M. Olszewski, W. Wolszczak

Laboratório de Instrumentação e Física Experimental de Partículas, Lisboa, Portugal

P. Bargassa, C. Beirão Da Cruz E Silva, P. Faccioli, P.G. Ferreira Parracho, M. Gallinaro, L. Lloret Iglesias, F. Nguyen, J. Rodrigues Antunes, J. Seixas, J. Varela, P. Vischia

Joint Institute for Nuclear Research, Dubna, Russia

I. Golutvin, I. Gorbunov, A. Kamenev, V. Karjavin, V. Konoplyanikov, G. Kozlov, A. Lanev, A. Malakhov, V. Matveev²⁹, P. Moisenz, V. Palichik, V. Pereygin, M. Savina, S. Shmatov, S. Shulha, N. Skatchkov, V. Smirnov, A. Zarubin

Petersburg Nuclear Physics Institute, Gatchina (St. Petersburg), Russia

V. Golovtsov, Y. Ivanov, V. Kim³⁰, P. Levchenko, V. Murzin, V. Oreshkin, I. Smirnov, V. Sulimov, L. Uvarov, S. Vavilov, A. Vorobyev, An. Vorobyev

Institute for Nuclear Research, Moscow, Russia

Yu. Andreev, A. Dermenev, S. Gninenko, N. Golubev, M. Kirsanov, N. Krasnikov, A. Pashenkov, D. Tlisov, A. Toropin

Institute for Theoretical and Experimental Physics, Moscow, Russia

V. Epshteyn, V. Gavrilov, N. Lychkovskaya, V. Popov, G. Safronov, S. Semenov, A. Spiridonov, V. Stolin, E. Vlasov, A. Zhokin

P.N. Lebedev Physical Institute, Moscow, Russia

V. Andreev, M. Azarkin, I. Dremin, M. Kirakosyan, A. Leonidov, G. Mesyats, S.V. Rusakov, A. Vinogradov

Skobeltsyn Institute of Nuclear Physics, Lomonosov Moscow State University, Moscow, Russia

A. Belyaev, E. Boos, V. Bunichev, M. Dubinin³¹, L. Dudko, A. Gribushin, V. Klyukhin, O. Kodolova, I. Lokhtin, S. Obraztsov, M. Perfilov, V. Savrin, A. Snigirev

State Research Center of Russian Federation, Institute for High Energy Physics, Protvino, Russia

I. Azhgirey, I. Bayshev, S. Bitioukov, V. Kachanov, A. Kalinin, D. Konstantinov, V. Krychkine, V. Petrov, R. Ryutin, A. Sobol, L. Tourtchanovitch, S. Troshin, N. Tyurin, A. Uzunian, A. Volkov

University of Belgrade, Faculty of Physics and Vinca Institute of Nuclear Sciences, Belgrade, Serbia

P. Adzic³², M. Ekmedzic, J. Milosevic, V. Rekovic

Centro de Investigaciones Energéticas Medioambientales y Tecnológicas (CIEMAT), Madrid, Spain

J. Alcaraz Maestre, C. Battilana, E. Calvo, M. Cerrada, M. Chamizo Llatas, N. Colino, B. De La Cruz, A. Delgado Peris, D. Domínguez Vázquez, A. Escalante Del Valle, C. Fernandez Bedoya, J.P. Fernández Ramos, J. Flix, M.C. Fouz, P. Garcia-Abia, O. Gonzalez Lopez, S. Goy Lopez, J.M. Hernandez, M.I. Josa, E. Navarro De Martino, A. Pérez-Calero Yzquierdo, J. Puerta Pelayo, A. Quintario Olmeda, I. Redondo, L. Romero, M.S. Soares

Universidad Autónoma de Madrid, Madrid, Spain

C. Albajar, J.F. de Trocóniz, M. Missiroli, D. Moran

Universidad de Oviedo, Oviedo, Spain

H. Brun, J. Cuevas, J. Fernandez Menendez, S. Folgueras, I. Gonzalez Caballero

Instituto de Física de Cantabria (IFCA), CSIC-Universidad de Cantabria, Santander, Spain

J.A. Brochero Cifuentes, I.J. Cabrillo, A. Calderon, J. Duarte Campderros, M. Fernandez, G. Gomez, A. Graziano, A. Lopez Virto, J. Marco, R. Marco, C. Martinez Rivero, F. Matorras, F.J. Munoz Sanchez, J. Piedra Gomez, T. Rodrigo, A.Y. Rodríguez-Marrero, A. Ruiz-Jimeno, L. Scodellaro, I. Vila, R. Vilar Cortabitarte

CERN, European Organization for Nuclear Research, Geneva, Switzerland

D. Abbaneo, E. Auffray, G. Auzinger, M. Bachtis, P. Baillon, A.H. Ball, D. Barney, A. Benaglia, J. Bendavid, L. Benhabib, J.F. Benitez, C. Bernet⁷, P. Bloch, A. Bocci, A. Bonato, O. Bondu, C. Botta, H. Breuker, T. Camporesi, G. Cerminara, S. Colafranceschi³³, M. D'Alfonso, D. d'Enterria, A. Dabrowski, A. David, F. De Guio, A. De Roeck, S. De Visscher, E. Di Marco, M. Dobson, M. Dordevic, B. Dorney, N. Dupont-Sagorin, A. Elliott-Peisert, J. Eugster, G. Franzoni, W. Funk, D. Gigi, K. Gill, D. Giordano, M. Girone, F. Glege, R. Guida, S. Gundacker, M. Guthoff, J. Hammer, M. Hansen, P. Harris, J. Hegeman, V. Innocente, P. Janot, K. Kousouris, K. Krajczar, P. Lecoq, C. Lourenço, N. Magini, L. Malgeri, M. Mannelli, J. Marrouche, L. Masetti, F. Meijers, S. Mersi, E. Meschi, F. Moortgat, S. Morovic, M. Mulders, P. Musella, L. Orsini, L. Pape, E. Perez, L. Perrozzi, A. Petrilli, G. Petrucciani, A. Pfeiffer, M. Pierini, M. Pimiä, D. Piparo, M. Plagge, A. Racz, G. Rolandi³⁴, M. Rovere, H. Sakulin, C. Schäfer, C. Schwick, A. Sharma, P. Siegrist, P. Silva, M. Simon, P. Sphicas³⁵, D. Spiga, J. Steggemann, B. Stieger, M. Stoye, Y. Takahashi, D. Treille, A. Tsiros, G.I. Veres¹⁷, N. Wardle, H.K. Wöhri, H. Wollny, W.D. Zeuner

Paul Scherrer Institut, Villigen, Switzerland

W. Bertl, K. Deiters, W. Erdmann, R. Horisberger, Q. Ingram, H.C. Kaestli, D. Kotlinski, U. Langenegger, D. Renker, T. Rohe

Institute for Particle Physics, ETH Zurich, Zurich, Switzerland

F. Bachmair, L. Bäni, L. Bianchini, M.A. Buchmann, B. Casal, N. Chanon, G. Dissertori, M. Dittmar, M. Donegà, M. Dünser, P. Eller, C. Grab, D. Hits, J. Hoss, W. Lustermann, B. Mangano, A.C. Marini, P. Martinez Ruiz del Arbol, M. Masciovecchio, D. Meister,

N. Mohr, C. Nägeli³⁶, F. Nessi-Tedaldi, F. Pandolfi, F. Pauss, M. Peruzzi, M. Quittnat, L. Rebane, M. Rossini, A. Starodumov³⁷, M. Takahashi, K. Theofilatos, R. Wallny, H.A. Weber

Universität Zürich, Zurich, Switzerland

C. Amsler³⁸, M.F. Canelli, V. Chiochia, A. De Cosa, A. Hinzmann, T. Hreus, B. Kilminster, C. Lange, B. Millan Mejias, J. Ngadiuba, P. Robmann, F.J. Ronga, S. Taroni, M. Verzetti, Y. Yang

National Central University, Chung-Li, Taiwan

M. Cardaci, K.H. Chen, C. Ferro, C.M. Kuo, W. Lin, Y.J. Lu, R. Volpe, S.S. Yu

National Taiwan University (NTU), Taipei, Taiwan

P. Chang, Y.H. Chang, Y.W. Chang, Y. Chao, K.F. Chen, P.H. Chen, C. Dietz, U. Grundler, W.-S. Hou, K.Y. Kao, Y.J. Lei, Y.F. Liu, R.-S. Lu, D. Majumder, E. Petrakou, Y.M. Tzeng, R. Wilken

Chulalongkorn University, Faculty of Science, Department of Physics, Bangkok, Thailand

B. Asavapibhop, G. Singh, N. Srimanobhas, N. Suwonjandee

Cukurova University, Adana, Turkey

A. Adiguzel, M.N. Bakirci³⁹, S. Cerci⁴⁰, C. Dozen, I. Dumanoglu, E. Eskut, S. Girgis, G. Gokbulut, E. Gurpinar, I. Hos, E.E. Kangal, A. Kayis Topaksu, G. Onengut⁴¹, K. Ozdemir, S. Ozturk³⁹, A. Polatoz, D. Sunar Cerci⁴⁰, B. Tali⁴⁰, H. Topakli³⁹, M. Vergili

Middle East Technical University, Physics Department, Ankara, Turkey

I.V. Akin, B. Bilin, S. Bilmis, H. Gamsizkan⁴², G. Karapinar⁴³, K. Ocalan⁴⁴, S. Sekmen, U.E. Surat, M. Yalvac, M. Zeyrek

Bogazici University, Istanbul, Turkey

E. Gülmez, B. Isildak⁴⁵, M. Kaya⁴⁶, O. Kaya⁴⁷

Istanbul Technical University, Istanbul, Turkey

K. Cankocak, F.I. Vardarli

National Scientific Center, Kharkov Institute of Physics and Technology, Kharkov, Ukraine

L. Levchuk, P. Sorokin

University of Bristol, Bristol, United Kingdom

J.J. Brooke, E. Clement, D. Cussans, H. Flacher, J. Goldstein, M. Grimes, G.P. Heath, H.F. Heath, J. Jacob, L. Kreczko, C. Lucas, Z. Meng, D.M. Newbold⁴⁸, S. Paramesvaran, A. Poll, S. Senkin, V.J. Smith, T. Williams

Rutherford Appleton Laboratory, Didcot, United Kingdom

K.W. Bell, A. Belyaev⁴⁹, C. Brew, R.M. Brown, D.J.A. Cockerill, J.A. Coughlan, K. Harder, S. Harper, E. Olaiya, D. Petyt, C.H. Shepherd-Themistocleous, A. Thea, I.R. Tomalin, W.J. Womersley, S.D. Worm

Imperial College, London, United Kingdom

M. Baber, R. Bainbridge, O. Buchmuller, D. Burton, D. Colling, N. Cripps, M. Cutajar, P. Dauncey, G. Davies, M. Della Negra, P. Dunne, W. Ferguson, J. Fulcher, D. Futyan, A. Gilbert, G. Hall, G. Iles, M. Jarvis, G. Karapostoli, M. Kenzie, R. Lane, R. Lucas⁴⁸, L. Lyons, A.-M. Magnan, S. Malik, B. Mathias, J. Nash, A. Nikitenko³⁷, J. Pela, M. Pesaresi, K. Petridis, D.M. Raymond, S. Rogerson, A. Rose, C. Seez, P. Sharp[†], A. Tapper, M. Vazquez Acosta, T. Virdee, S.C. Zenz

Brunel University, Uxbridge, United Kingdom

J.E. Cole, P.R. Hobson, A. Khan, P. Kyberd, D. Leggat, D. Leslie, W. Martin, I.D. Reid, P. Symonds, L. Teodorescu, M. Turner

Baylor University, Waco, USA

J. Dittmann, K. Hatakeyama, A. Kasmi, H. Liu, T. Scarborough

The University of Alabama, Tuscaloosa, USA

O. Charaf, S.I. Cooper, C. Henderson, P. Rumerio

Boston University, Boston, USA

A. Avetisyan, T. Bose, C. Fantasia, P. Lawson, C. Richardson, J. Rohlf, J. St. John, L. Sulak

Brown University, Providence, USA

J. Alimena, E. Berry, S. Bhattacharya, G. Christopher, D. Cutts, Z. Demiragli, N. Dhirga, A. Ferapontov, A. Garabedian, U. Heintz, G. Kukartsev, E. Laird, G. Landsberg, M. Luk, M. Narain, M. Segala, T. Sinthuprasith, T. Speer, J. Swanson

University of California, Davis, Davis, USA

R. Breedon, G. Breto, M. Calderon De La Barca Sanchez, S. Chauhan, M. Chertok, J. Conway, R. Conway, P.T. Cox, R. Erbacher, M. Gardner, W. Ko, R. Lander, T. Miceli, M. Mulhearn, D. Pellett, J. Pilot, F. Ricci-Tam, M. Searle, S. Shalhout, J. Smith, M. Squires, D. Stolp, M. Tripathi, S. Wilbur, R. Yohay

University of California, Los Angeles, USA

R. Cousins, P. Everaerts, C. Farrell, J. Hauser, M. Ignatenko, G. Rakness, E. Takasugi, V. Valuev, M. Weber

University of California, Riverside, Riverside, USA

K. Burt, R. Clare, J. Ellison, J.W. Gary, G. Hanson, J. Heilman, M. Ivova Rikova, P. Jandir, E. Kennedy, F. Lacroix, O.R. Long, A. Luthra, M. Malberti, H. Nguyen, M. Olmedo Negrete, A. Shrinivas, S. Sumowidagdo, S. Wimpenny

University of California, San Diego, La Jolla, USA

W. Andrews, J.G. Branson, G.B. Cerati, S. Cittolin, R.T. D'Agnolo, D. Evans, A. Holzner, R. Kelley, D. Klein, M. Lebourgeois, J. Letts, I. Macneill, D. Olivito, S. Padhi, C. Palmer, M. Pieri, M. Sani, V. Sharma, S. Simon, E. Sudano, M. Tadel, Y. Tu, A. Vartak, C. Welke, F. Wüthwein, A. Yagil

University of California, Santa Barbara, Santa Barbara, USA

D. Barge, J. Bradmiller-Feld, C. Campagnari, T. Danielson, A. Dishaw, V. Dutta, K. Flowers, M. Franco Sevilla, P. Geffert, C. George, F. Golf, L. Gouskos, J. Incandela, C. Justus, N. Mccoll, J. Richman, D. Stuart, W. To, C. West, J. Yoo

California Institute of Technology, Pasadena, USA

A. Apresyan, A. Bornheim, J. Bunn, Y. Chen, J. Duarte, A. Mott, H.B. Newman, C. Pena, C. Rogan, M. Spiropulu, V. Timciuc, J.R. Vlimant, R. Wilkinson, S. Xie, R.Y. Zhu

Carnegie Mellon University, Pittsburgh, USA

V. Azzolini, A. Calamba, B. Carlson, T. Ferguson, Y. Iiyama, M. Paulini, J. Russ, H. Vogel, I. Vorobiev

University of Colorado at Boulder, Boulder, USA

J.P. Cumalat, W.T. Ford, A. Gaz, E. Luiggi Lopez, U. Nauenberg, J.G. Smith, K. Stenson, K.A. Ulmer, S.R. Wagner

Cornell University, Ithaca, USA

J. Alexander, A. Chatterjee, J. Chu, S. Dittmer, N. Eggert, N. Mirman, G. Nicolas Kaufman, J.R. Patterson, A. Ryd, E. Salvati, L. Skinnari, W. Sun, W.D. Teo, J. Thom, J. Thompson, J. Tucker, Y. Weng, L. Winstrom, P. Wittich

Fairfield University, Fairfield, USA

D. Winn

Fermi National Accelerator Laboratory, Batavia, USA

S. Abdullin, M. Albrow, J. Anderson, G. Apollinari, L.A.T. Bauerdick, A. Beretvas, J. Berryhill, P.C. Bhat, G. Bolla, K. Burkett, J.N. Butler, H.W.K. Cheung, F. Chlebana, S. Cihangir, V.D. Elvira, I. Fisk, J. Freeman, Y. Gao, E. Gottschalk, L. Gray, D. Green, S. Grünendahl, O. Gutsche, J. Hanlon, D. Hare, R.M. Harris, J. Hirschauer, B. Hooberman, S. Jindariani, M. Johnson, U. Joshi, K. Kaadze, B. Klima, B. Kreis, S. Kwan, J. Linacre, D. Lincoln, R. Lipton, T. Liu, J. Lykken, K. Maeshima, J.M. Marraffino, V.I. Martinez Outschoorn, S. Maruyama, D. Mason, P. McBride, P. Merkel, K. Mishra, S. Mrenna, Y. Musienko²⁹, S. Nahn, C. Newman-Holmes, V. O'Dell, O. Prokofyev, E. Sexton-Kennedy, S. Sharma, A. Soha, W.J. Spalding, L. Spiegel, L. Taylor, S. Tkaczyk, N.V. Tran, L. Uplegger, E.W. Vaandering, R. Vidal, A. Whitbeck, J. Whitmore, F. Yang

University of Florida, Gainesville, USA

D. Acosta, P. Avery, P. Bortignon, D. Bourilkov, M. Carver, T. Cheng, D. Curry, S. Das, M. De Gruttola, G.P. Di Giovanni, R.D. Field, M. Fisher, I.K. Furic, J. Hugon, J. Konigsberg, A. Korytov, T. Kypreos, J.F. Low, K. Matchev, P. Milenovic⁵⁰, G. Mitselmakher, L. Muniz, A. Rinkevicius, L. Shchutska, M. Snowball, D. Sperka, J. Yelton, M. Zakaria

Florida International University, Miami, USA

S. Hewamanage, S. Linn, P. Markowitz, G. Martinez, J.L. Rodriguez

Florida State University, Tallahassee, USA

T. Adams, A. Askew, J. Bochenek, B. Diamond, J. Haas, S. Hagopian, V. Hagopian, K.F. Johnson, H. Prosper, V. Veeraraghavan, M. Weinberg

Florida Institute of Technology, Melbourne, USA

M.M. Baarmand, M. Hohlmann, H. Kalakhety, F. Yumiceva

University of Illinois at Chicago (UIC), Chicago, USA

M.R. Adams, L. Apanasevich, V.E. Bazterra, D. Berry, R.R. Betts, I. Bucinskaite, R. Cavanaugh, O. Evdokimov, L. Gauthier, C.E. Gerber, D.J. Hofman, S. Khalatyan, P. Kurt, D.H. Moon, C. O'Brien, C. Silkworth, P. Turner, N. Varelas

The University of Iowa, Iowa City, USA

E.A. Albayrak⁵¹, B. Bilki⁵², W. Clarida, K. Dilsiz, F. Duru, M. Haytmyradov, J.-P. Merlo, H. Mermerkaya⁵³, A. Mestvirishvili, A. Moeller, J. Nachtman, H. Ogul, Y. Onel, F. Ozok⁵¹, A. Penzo, R. Rahmat, S. Sen, P. Tan, E. Tiras, J. Wetzel, T. Yetkin⁵⁴, K. Yi

Johns Hopkins University, Baltimore, USA

B.A. Barnett, B. Blumenfeld, S. Bolognesi, D. Fehling, A.V. Gritsan, P. Maksimovic, C. Martin, M. Swartz

The University of Kansas, Lawrence, USA

P. Baringer, A. Bean, G. Benelli, C. Bruner, R.P. Kenny III, M. Malek, M. Murray, D. Noonan, S. Sanders, J. Sekaric, R. Stringer, Q. Wang, J.S. Wood

Kansas State University, Manhattan, USA

I. Chakaberia, A. Ivanov, S. Khalil, M. Makouski, Y. Maravin, L.K. Saini, S. Shrestha, N. Skhirtladze, I. Svintradze

Lawrence Livermore National Laboratory, Livermore, USA

J. Gronberg, D. Lange, F. Rebassoo, D. Wright

University of Maryland, College Park, USA

A. Baden, A. Belloni, B. Calvert, S.C. Eno, J.A. Gomez, N.J. Hadley, R.G. Kellogg, T. Kolberg, Y. Lu, M. Marionneau, A.C. Mignerey, K. Pedro, A. Skuja, M.B. Tonjes, S.C. Tonwar

Massachusetts Institute of Technology, Cambridge, USA

A. Apyan, R. Barbieri, G. Bauer, W. Busza, I.A. Cali, M. Chan, L. Di Matteo, G. Gomez Ceballos, M. Goncharov, D. Gulhan, M. Klute, Y.S. Lai, Y.-J. Lee, A. Levin, P.D. Luckey, T. Ma, C. Paus, D. Ralph, C. Roland, G. Roland, G.S.F. Stephans, F. Stöckli, K. Sumorok, D. Velicanu, J. Veverka, B. Wyslouch, M. Yang, M. Zanetti, V. Zhukova

University of Minnesota, Minneapolis, USA

B. Dahmes, A. Gude, S.C. Kao, K. Klapoetke, Y. Kubota, J. Mans, N. Pastika, R. Rusack, A. Singovsky, N. Tambe, J. Turkewitz

University of Mississippi, Oxford, USA

J.G. Acosta, S. Oliveros

University of Nebraska-Lincoln, Lincoln, USA

E. Avdeeva, K. Bloom, S. Bose, D.R. Claes, A. Dominguez, R. Gonzalez Suarez, J. Keller, D. Knowlton, I. Kravchenko, J. Lazo-Flores, S. Malik, F. Meier, G.R. Snow, M. Zvada

State University of New York at Buffalo, Buffalo, USA

J. Dolen, A. Godshalk, I. Iashvili, A. Kharchilava, A. Kumar, S. Rappoccio

Northeastern University, Boston, USA

G. Alverson, E. Barberis, D. Baumgartel, M. Chasco, J. Haley, A. Massironi, D.M. Morse, D. Nash, T. Orimoto, D. Trocino, R.-J. Wang, D. Wood, J. Zhang

Northwestern University, Evanston, USA

K.A. Hahn, A. Kubik, N. Mucia, N. Odell, B. Pollack, A. Pozdnyakov, M. Schmitt, S. Stoynev, K. Sung, M. Velasco, S. Won

University of Notre Dame, Notre Dame, USA

A. Brinkerhoff, K.M. Chan, A. Drozdetskiy, M. Hildreth, C. Jessop, D.J. Karmgard, N. Kellams, K. Lannon, W. Luo, S. Lynch, N. Marinelli, T. Pearson, M. Planer, R. Ruchti, N. Valls, M. Wayne, M. Wolf, A. Woodard

The Ohio State University, Columbus, USA

L. Antonelli, J. Brinson, B. Bylsma, L.S. Durkin, S. Flowers, A. Hart, C. Hill, R. Hughes, K. Kotov, T.Y. Ling, D. Puigh, M. Rodenburg, G. Smith, B.L. Winer, H. Wolfe, H.W. Wulsin

Princeton University, Princeton, USA

O. Driga, P. Elmer, P. Hebda, A. Hunt, S.A. Koay, P. Lujan, D. Marlow, T. Medvedeva, M. Mooney, J. Olsen, P. Piroué, X. Quan, H. Saka, D. Stickland², C. Tully, J.S. Werner, A. Zuranski

University of Puerto Rico, Mayaguez, USA

E. Brownson, H. Mendez, J.E. Ramirez Vargas

Purdue University, West Lafayette, USA

V.E. Barnes, D. Benedetti, D. Bortoletto, M. De Mattia, L. Gutay, Z. Hu, M.K. Jha, M. Jones, K. Jung, M. Kress, N. Leonardo, D. Lopes Pegna, V. Maroussov, D.H. Miller, N. Neumeister, B.C. Radburn-Smith, X. Shi, I. Shipsey, D. Silvers, A. Svyatkovskiy, F. Wang, W. Xie, L. Xu, J. Zablocki, Y. Zheng

Purdue University Calumet, Hammond, USA

N. Parashar, J. Stupak

Rice University, Houston, USA

A. Adair, B. Akgun, K.M. Ecklund, F.J.M. Geurts, W. Li, B. Michlin, B.P. Padley, R. Redjimi, J. Roberts, J. Zabel

University of Rochester, Rochester, USA

B. Betchart, A. Bodek, R. Covarelli, P. de Barbaro, R. Demina, Y. Eshaq, T. Ferbel, A. Garcia-Bellido, P. Goldenzweig, J. Han, A. Harel, A. Khukhunaishvili, G. Petrillo, D. Vishnevskiy

The Rockefeller University, New York, USA

R. Ciesielski, L. Demortier, K. Goulianos, G. Lungu, C. Mesropian

Rutgers, The State University of New Jersey, Piscataway, USA

S. Arora, A. Barker, J.P. Chou, C. Contreras-Campana, E. Contreras-Campana, D. Dugan, D. Ferencek, Y. Gershtein, R. Gray, E. Halkiadakis, D. Hidas, S. Kaplan, A. Lath, S. Panwalkar, M. Park, R. Patel, S. Salur, S. Schnetzer, S. Somalwar, R. Stone, S. Thomas, P. Thomassen, M. Walker

University of Tennessee, Knoxville, USA

K. Rose, S. Spanier, A. York

Texas A&M University, College Station, USA

O. Bouhali⁵⁵, A. Castaneda Hernandez, R. Eusebi, W. Flanagan, J. Gilmore, T. Kamon⁵⁶, V. Khotilovich, V. Krutelyov, R. Montalvo, I. Osipenkov, Y. Pakhotin, A. Perloff, J. Roe, A. Rose, A. Safonov, T. Sakuma, I. Suarez, A. Tatarinov

Texas Tech University, Lubbock, USA

N. Akchurin, C. Cowden, J. Damgov, C. Dragoiu, P.R. Dudero, J. Faulkner, K. Kovitangoon, S. Kunori, S.W. Lee, T. Libeiro, I. Volobouev

Vanderbilt University, Nashville, USA

E. Appelt, A.G. Delannoy, S. Greene, A. Gurrola, W. Johns, C. Maguire, Y. Mao, A. Melo, M. Sharma, P. Sheldon, B. Snook, S. Tuo, J. Velkovska

University of Virginia, Charlottesville, USA

M.W. Arenton, S. Boutle, B. Cox, B. Francis, J. Goodell, R. Hirosky, A. Ledovskoy, H. Li, C. Lin, C. Neu, J. Wood

Wayne State University, Detroit, USA

C. Clarke, R. Harr, P.E. Karchin, C. Kottachchi Kankanamge Don, P. Lamichhane, J. Sturdy

University of Wisconsin, Madison, USA

D.A. Belknap, D. Carlsmith, M. Cepeda, S. Dasu, L. Dodd, S. Duric, E. Friis, R. Hall-Wilton, M. Herndon, A. Hervé, P. Klabbers, A. Lanaro, C. Lazaridis, A. Levine, R. Lovelless, A. Mohapatra, I. Ojalvo, T. Perry, G.A. Pierro, G. Polese, I. Ross, T. Sarangi, A. Savin, W.H. Smith, D. Taylor, P. Verwilligen, C. Vuosalo, N. Woods

†: Deceased

1: Also at Vienna University of Technology, Vienna, Austria

2: Also at CERN, European Organization for Nuclear Research, Geneva, Switzerland

- 3: Also at Institut Pluridisciplinaire Hubert Curien, Université de Strasbourg, Université de Haute Alsace Mulhouse, CNRS/IN2P3, Strasbourg, France
- 4: Also at National Institute of Chemical Physics and Biophysics, Tallinn, Estonia
- 5: Also at Skobeltsyn Institute of Nuclear Physics, Lomonosov Moscow State University, Moscow, Russia
- 6: Also at Universidade Estadual de Campinas, Campinas, Brazil
- 7: Also at Laboratoire Leprince-Ringuet, Ecole Polytechnique, IN2P3-CNRS, Palaiseau, France
- 8: Also at Joint Institute for Nuclear Research, Dubna, Russia
- 9: Also at Suez University, Suez, Egypt
- 10: Also at British University in Egypt, Cairo, Egypt
- 11: Also at Fayoum University, El-Fayoum, Egypt
- 12: Also at Ain Shams University, Cairo, Egypt
- 13: Now at Sultan Qaboos University, Muscat, Oman
- 14: Also at Université de Haute Alsace, Mulhouse, France
- 15: Also at Brandenburg University of Technology, Cottbus, Germany
- 16: Also at Institute of Nuclear Research ATOMKI, Debrecen, Hungary
- 17: Also at Eötvös Loránd University, Budapest, Hungary
- 18: Also at University of Debrecen, Debrecen, Hungary
- 19: Also at University of Visva-Bharati, Santiniketan, India
- 20: Now at King Abdulaziz University, Jeddah, Saudi Arabia
- 21: Also at University of Ruhuna, Matara, Sri Lanka
- 22: Also at Isfahan University of Technology, Isfahan, Iran
- 23: Also at University of Tehran, Department of Engineering Science, Tehran, Iran
- 24: Also at Plasma Physics Research Center, Science and Research Branch, Islamic Azad University, Tehran, Iran
- 25: Also at Università degli Studi di Siena, Siena, Italy
- 26: Also at Centre National de la Recherche Scientifique (CNRS) - IN2P3, Paris, France
- 27: Also at Purdue University, West Lafayette, USA
- 28: Also at Universidad Michoacana de San Nicolas de Hidalgo, Morelia, Mexico
- 29: Also at Institute for Nuclear Research, Moscow, Russia
- 30: Also at St. Petersburg State Polytechnical University, St. Petersburg, Russia
- 31: Also at California Institute of Technology, Pasadena, USA
- 32: Also at Faculty of Physics, University of Belgrade, Belgrade, Serbia
- 33: Also at Facoltà Ingegneria, Università di Roma, Roma, Italy
- 34: Also at Scuola Normale e Sezione dell'INFN, Pisa, Italy
- 35: Also at University of Athens, Athens, Greece
- 36: Also at Paul Scherrer Institut, Villigen, Switzerland
- 37: Also at Institute for Theoretical and Experimental Physics, Moscow, Russia
- 38: Also at Albert Einstein Center for Fundamental Physics, Bern, Switzerland
- 39: Also at Gaziosmanpasa University, Tokat, Turkey
- 40: Also at Adiyaman University, Adiyaman, Turkey
- 41: Also at Cag University, Mersin, Turkey
- 42: Also at Anadolu University, Eskisehir, Turkey
- 43: Also at Izmir Institute of Technology, Izmir, Turkey
- 44: Also at Necmettin Erbakan University, Konya, Turkey
- 45: Also at Ozyegin University, Istanbul, Turkey
- 46: Also at Marmara University, Istanbul, Turkey
- 47: Also at Kafkas University, Kars, Turkey

- 48: Also at Rutherford Appleton Laboratory, Didcot, United Kingdom
- 49: Also at School of Physics and Astronomy, University of Southampton, Southampton, United Kingdom
- 50: Also at University of Belgrade, Faculty of Physics and Vinca Institute of Nuclear Sciences, Belgrade, Serbia
- 51: Also at Mimar Sinan University, Istanbul, Istanbul, Turkey
- 52: Also at Argonne National Laboratory, Argonne, USA
- 53: Also at Erzincan University, Erzincan, Turkey
- 54: Also at Yildiz Technical University, Istanbul, Turkey
- 55: Also at Texas A&M University at Qatar, Doha, Qatar
- 56: Also at Kyungpook National University, Daegu, Korea